



ELSEVIER

Available online at www.sciencedirect.com

Remote Sensing of Environment xx (2007) xxx–xxx

Remote Sensing
of
Environment

www.elsevier.com/locate/rse

Mapping tree and shrub leaf area indices in an ombrotrophic peatland through multiple endmember spectral unmixing

O. Sonnentag^{a,*}, J.M. Chen^{a,1}, D.A. Roberts^{b,2}, J. Talbot^{c,3}, K.Q. Halligan^{b,2}, A. Govind^{a,1}

^a University of Toronto, Department of Geography and Planning, St. George Campus, Sidney Smith Hall, 100 St. George St., Room 5047, Toronto, ON, Canada M5S 3G3

^b University of California Santa Barbara, Department of Geography, 3611 Ellison Hall, Santa Barbara, CA, 93106-4060, USA

^c McGill University, Department of Geography, Burnside Hall, 805 Sherbrooke West, Room 705, Montreal, QC, Canada H3A 2K6

Received 12 October 2006; received in revised form 8 January 2007; accepted 13 January 2007

Abstract

Leaf area index (LAI) is an important parameter used by most process-oriented ecosystem models. LAI of forest ecosystems has routinely been mapped using spectral vegetation indices (SVI) derived from remote sensing imagery. The application of SVI-based approaches to map LAI in peatlands presents a challenge, mainly due to peatlands characteristic multi-layer canopy comprising shrubs and open, discontinuous tree canopies underlain by a continuous ground cover of different moss species, which reduces the greenness contrast between the canopy and the background.

Our goal is to develop a methodology to map tree and shrub LAI in peatlands and similar ecosystems based on multiple endmember spectral mixture analysis (MESMA). This new mapping method is validated using LAI field measurements from a precipitation-fed (ombrotrophic) peatland near Ottawa, Ontario, Canada. We demonstrate first that three commonly applied SVI are not suitable for tree and shrub LAI mapping in ombrotrophic peatlands. Secondly, we demonstrate for a three-endmember model the limitations of traditional linear spectral mixture analysis (SMA) due to the unique and widely varying spectral characteristics of *Sphagnum* mosses, which are significantly different from vascular plants. Next, by using a geometric-optical radiative transfer model, we determine the nature of the equation describing the empirical relationship between shadow fraction and tree LAI using nonlinear ordinary least square (OLS) regression. We then apply this equation to describe the empirical relationships between shadow and shrub fractions obtained from mixture decomposition with SMA and MESMA, respectively, and tree and shrub LAI, respectively. Less accurate fractions obtained from SMA result in weaker relationships between shadow fraction and tree LAI ($R^2=0.61$) and shrub fraction and shrub LAI ($R^2=0.49$) compared to the same relationships based on fractions obtained from MESMA with $R^2=0.75$ and $R^2=0.68$, respectively. Cross-validation of tree LAI ($R^2=0.74$; RMSE=0.48) and shrub LAI ($R^2=0.68$; RMSE=0.42) maps using fractions from MESMA shows the suitability of this approach for mapping tree and shrub LAI in ombrotrophic peatlands. The ability to account for a spectrally varying, unique *Sphagnum* moss ground cover during mixture decomposition and a two layer canopy is particularly important.

© 2007 Elsevier Inc. All rights reserved.

Keywords: Leaf area index; LAI-2000; Peatlands; Spectral mixture analysis; SMA; MESMA

1. Introduction

Peatlands, which are wetlands that accumulate partially decayed plant matter as peat, are an extensive component of boreal and subarctic ecozones. In Canada, they cover about 14%

of the land area (Tarnocai et al., 2000). Bogs are common types of peatlands which are precipitation-fed (ombrotrophic) and generally lack any other hydrological inputs, resulting in acidic and nutrient-poor conditions. The characteristic multi-layer canopy of bogs comprises a *Sphagnum* moss ground cover under ericaceous shrubs, and patches of sparse coniferous trees. Due to this vertical vegetation structure, a substantial proportion of the solar energy reaches the shrub canopy resulting in a significant role for shrubs in carbon, water, and energy exchanges with the atmosphere (e.g., Baldocchi et al., 2000; Lafleur et al., 2005; Moore et al., 2002).

* Corresponding author. Tel.: +1 416 946 7715; fax: +1 416 946 3886.

E-mail address: oliver.sonnentag@utoronto.ca (O. Sonnentag).

¹ Tel.: +1 416 946 7715; fax: +1 416 946 3886.

² Tel.: +1 805 893 2276.

³ Tel.: +1 514 398 4111.

Peat accumulation is the result of net primary productivity (NPP), the net gain of carbon in the form of biomass through photosynthesis, persistently exceeding the decomposition of organic matter. Peatlands act as long term stores of carbon with an average long-term apparent carbon accumulation rate of 15–30 g C m⁻² year⁻¹ (Turunen et al., 2002). As a result, peatlands store up to 450 Gt C or one third of the global soil carbon (Gorham, 1991; Turunen et al., 2002). The role of peatlands as long-term carbon sinks in the global carbon cycle is closely related to climatic conditions. Possible responses of peatlands to climatic changes might include shifts in peatland distribution and extent, and a switch from long-term sinks to long-term sources of atmospheric carbon (e.g., Gorham, 1991; Moore et al., 1998).

A promising means to quantify possible responses of peatland carbon dynamics to likely climatic changes is the use of process-oriented ecosystem models as predictive tools. An important parameter of most process-oriented ecosystem models is the leaf area index (LAI). LAI is a dimensionless quantity of the amount of foliage area of a vegetation canopy and is defined as one half the total leaf area (all-sided) per unit ground horizontal surface area (Chen & Black, 1992). LAI characterizes the canopy–atmosphere interface of an ecosystem, and is therefore related to precipitation and atmospheric nutrient deposition interception, canopy microclimate, radiation extinction, and water, carbon, and energy exchanges with the atmosphere. Some process-oriented models such as the Boreal Ecosystem Productivity Simulator (BEPS; Liu et al., 1997) use LAI as an input parameter, while others such as the Peatland Carbon Simulator (PCARS; Frohling et al., 2002) generate LAI as a function of foliar biomass. For the parameterization of distributed, process-oriented ecosystem models such as BEPS, tree LAI in forest ecosystems has traditionally been mapped based on ordinary least square (OLS) regression analysis relationships between field-measured tree LAI and various spectral vegetation indices (SVI) derived from remote sensing imagery. Common SVI used for this purpose are the normalized difference vegetation index (NDVI; Deering, 1978), [(NIR – red)/(NIR + red)], the simple ratio (SR; Jordan, 1969), [NIR/red], and the reduced simple ratio (RSR; Brown et al., 2000), [SR * (1 – (SWIR – SWIR_{min})/(SWIR_{max} – SWIR_{min}))] (Chen & Cihlar, 1996; Chen et al., 2002; Eklundh et al., 2003). However, the multi-layer canopy of ombrotrophic peatlands limits the applicability of SVI-based approaches to map tree LAI due to the discontinuity and openness of the tree canopy consisting of spatially distinct crowns resulting in increased shadow fraction, and due to the reduced greenness contrast between the canopy and the background.

Background reflectance in ombrotrophic peatlands varies depending on the vertical vegetation structure within the peatland. In forested portions, sunlit trees are the principal contributor to the overall spectral response. The background reflectance, mainly determined by crown closure, is composed of the spectral reflectance of tree and shrub shadow on neighbouring trees, shrubs, and mosses, sunlit shrubs and mosses, and, in places, open water. In open portions where trees are absent, sunlit shrubs are the principal contributors to the overall spectral response. Here, the background reflectance, mainly determined by shrub canopy closure, is composed of shrub shadow on neighbouring shrubs

and mosses, sunlit mosses, and, in places, open water. Thus, in both forested and open portions, the background reflectance contributing to the overall spectral response is partially controlled by the spectral characteristics of mosses, which are significantly different from vascular plants in the visible, NIR, and short-wave infrared (SWIR) ranges of the electromagnetic spectrum (Bubier et al., 1997).

Alternative approaches to map tree LAI in forest ecosystems based on remote sensing imagery include the application of inverse OLS and reduced major axis (RMA) regression analysis, and geostatistical techniques such as cokriging, kriging with external drift (KED), and sequential Gaussian conditional simulation (SGCS) (Berterreche et al., 2005; Cohen et al., 2003). Another promising route to map tree LAI in forest ecosystems was proposed by Hall et al. (1995). In their study they demonstrated empirically and theoretically that the scene fractions of shadow and sunlit background obtained by mixture decomposition of a three-endmember model (sunlit tree canopy, sunlit background, and shadow) with linear spectral mixture analysis (SMA) were related to biophysical parameters such as LAI. The dependence of these fractions on solar zenith angle < 50° (SZA) was shown to be minimal. SMA-based approaches to map tree LAI were also pursued by Hall et al. (2003), Hu et al. (2004), and Peddle et al. (1999).

Considering the importance of the shrub canopy in the overall hydrological and ecological functioning of peatlands, its reliable parameterization in distributed, process-oriented ecosystem models in addition to the tree canopy is mandatory. However, none of the existing remote sensing-based methods allows for the separate mapping of tree and shrub LAI of a multi-layer canopy comprising shrubs and open, discontinuous tree canopies. Our goal was to develop a methodology for tree and shrub LAI mapping in ombrotrophic peatlands and similar ecosystems based on field measurements, geometric-optical radiative transfer modelling, and multiple endmember spectral mixture analysis (MESMA; Roberts et al., 1998). MESMA is an extension of SMA that takes into account the spectral variability within endmembers and optionally allows the number of endmembers to vary on a per-pixel basis. To achieve our goal we carefully quantified tree and shrub LAI during peak growing season in the Mer Bleue bog using the LAI-2000 plant canopy analyzer. This included the determination of previously unavailable species-specific LAI-2000 correction factors for tamarack. The multi-layer canopy of the bog and its species composition are typical for ombrotrophic peatlands (Payette & Rochefort, 2001). Furthermore, we tested the applicability of NDVI, SR, and RSR for tree and shrub LAI mapping, and demonstrated the superiority of MESMA over SMA in ombrotrophic peatlands due to the unique and widely varying spectral characteristics of *Sphagnum* mosses.

2. Materials and methods

2.1. Site description and transect locations

The Mer Bleue bog (45.4°N latitude, 75.5°W longitude) is a raised, ombrotrophic peatland, about 10 km south-east of

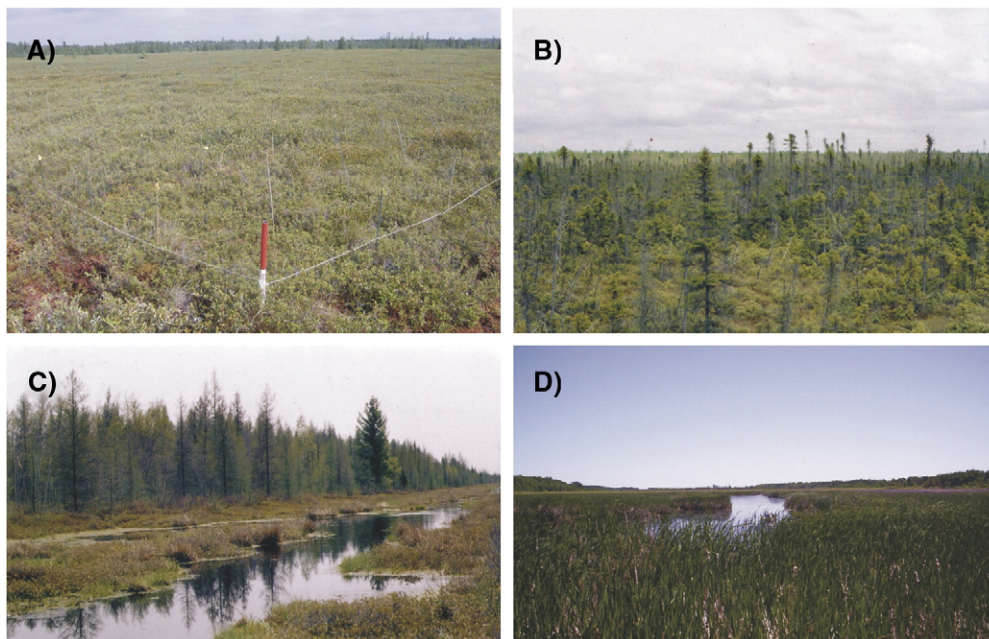


Fig. 1. Dominant species composition and vegetation structures occurring at Mer Bleu: A) pristine shrub canopy comprising evergreen and deciduous shrubs, B) sparse patches of pristine tree canopy comprising mainly tamarack and black spruce, C) relatively dense mixed tree canopy along a drainage ditch, and D) mineral wetland (marsh) comprising mainly cattail (the approximate locations of all photographs are given in Fig. 2).

158 Ottawa, Ontario, Canada. It covers an area of about 28 km² and
 159 is roughly oval shaped with an east–west orientation. The
 160 climate of the region is cool continental, with a 30-year (1971–
 161 2000) mean annual temperature of 6.0±0.8 °C. Sub-surface
 162 water and sometimes surface water is shed from the gently
 163 domed central part of the bog towards its margins, where it
 164 drains away along beaver ponds surrounding the bog (Roulet
 165 et al., 2006). The pristine (undisturbed) species composition of
 166 Mer Bleu bog is characterized by dominant evergreen shrubs
 167 (*Chamaedaphne calyculata*, *Ledum groenlandicum*, *Kalmia*
 168 *angustifolia*, *Kalmia polifolia*, *Andromeda glaucophylla*), decid-
 169 uous shrubs (*Vaccinium myrtilloides*) (Fig. 1A), and sparse
 170 patches of sedges (*Eriophorum spissum*), black spruce (*Picea*
 171 *mariana*) and tamarack (*Larix laricina*) trees, and occasion-
 172 al grey birch (*Betula populifolia*) and white birch (*Betula*
 173 *papyrifera*) trees (Fig. 1B). The average canopy height is
 174 about 0.20 m and 3 m for the shrub and sparse tree canopy,
 175 respectively. The surface of the bog is covered by species of
 176 *Sphagnum* moss (*Sp. angustifolium*, *Sp. capillifolium*,
 177 *Sp. magellanicum*, and *Sp. fuscum*). Characteristic features of
 178 the bog are distinct microforms consisting of hollows, hum-
 179 mucks, and intermediate lawns, with a mean relief between
 180 hollows and hummocks of 0.25 m (Lafleur et al., 2005).

181 The species composition along narrow bands of several
 182 approximately north–south oriented drainage ditches is char-
 183 acterized by a relatively dense mixed tree canopy that consists
 184 primarily of tamarack and grey birch with interspersed black
 185 spruce and white pine (*Pinus strobus*) (Fig. 1C). The average
 186 tree canopy height is about 10 m. The species composition of
 187 the shrub canopy in these areas is the same as for the rest of
 188 the bog, but reaches an average height of 1 m. The patchy

ground cover is composed of *Sphagnum* and brown mosses. 189
 This vertical vegetation structure reflects the drained condi- 190
 tions along drainage ditches and in the transition between the 191
 peat body and surrounding mineral wetlands (cattail marsh). 192
 The cattail marshes are dominated by narrow-leaved cattail 193
 (*Typha angustifolia*) with an average height of about 2.5 m 194
 (Fig. 1D). In the following we use “Mer Bleu bog” to refer to 195
 the ombrotrophic peatland characterized by pristine species 196
 composition and vertical vegetation structure, whereas “Mer 197
 Bleu” is used to refer to the ombrotrophic peatland and the 198
 surrounding mineral wetlands as defined by the National 199
 Capital Commission (Ottawa, Ontario, Canada) (Fig. 2). 200

Using the LAI-2000 plant canopy analyzer (Norman & 201
 Welles, 1991; Li-COR, Lincoln, Nebraska, USA), we mea- 202
 sured tree LAI along five transects (mbt1, mbt2, mbt3, mbt4, 203
 and mbt5) and shrub LAI along eight transects (mbt1, mbt2, 204

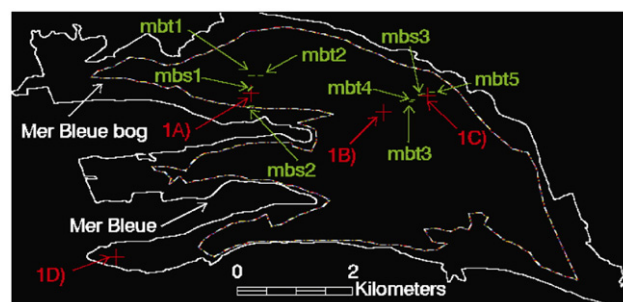


Fig. 2. Transect (green) and approximate photograph (red) locations of Fig. 1 within Mer Bleu (after National Capitol Commission, Ottawa, Ontario, Canada) and Mer Bleu bog (approximate boundary).

Transect	Length [m]	Orientation	Species composition	
t1.4	mbt1	100	E–W	Tamarack/mixed shrubs
t1.5	mbt2	100	E–W	Black spruce/mixed shrubs
t1.6	mbt3	50	~E–W	Tamarack/black spruce/mixed shrubs
t1.7	mbt4	50	~E–W	Tamarack/black spruce/mixed shrubs
t1.8	mbt5	100	E–W	Mixed forest/mixed shrubs (d)
t1.9	mbs1	100	NE–SW	Mixed shrubs
t1.10	mbs2	100	NE–SW	Mixed shrubs
t1.11	mbs3	100	NE–SW	Mixed shrubs

mbt3, mbt4, mbt5, mbs1, mbs2, and mbs3) in August 2005 (Fig. 2).

All transects were 50 m or 100 m in length, and oriented in northeast–southwest or east–west direction (Table 1). Along each transect a forestry flag was placed every 10 m to serve as a distance marker. The positions of all flags were recorded in UTM coordinates (North American Datum 1983) using a GPSMAP76 global positioning system (Garmin International Inc., Olathe, KS, USA).

For the tree transects, basal area and stand density (just for mbt3, mbt4, and mbt5), and for the shrub transects, species composition and percent cover, were estimated at each flag position (within a 50 × 50 cm plot with the flag in the center) prior to the LAI-2000 measurements.

2.2. LAI field and laboratory measurements

The LAI-2000 instrument measures canopy gap fractions by detecting blue diffuse light (between 400 and 490 nm) penetrating the canopy with quantum detectors arranged in five concentric rings. The LAI estimate obtained from the LAI-2000 instrument is an “effective” LAI (LAI_e) derived from the light interception of all canopy elements using a radiative transfer model (Chen, 1996; Chen et al., 1997).

All LAI-2000 measurements were taken at dusk or dawn, i.e. under diffuse sky conditions, to minimize the effect of multiple scattering of light within the canopies and to prevent direct sunlight on the instrument sensor. To avoid any effects of the operator on the instrument sensor, a 270° view cap was used for all measurements. The post-processing of all measurements was accomplished using the LAI-2000 analysis software provided by LI-COR (F2000.exe). As part of the post-processing, the outer two rings of the quantum sensor were excluded from the final calculation of LAI_e to (i) decrease the influence of stronger multiple light scattering effects at larger zenith angles (Chen et al., 2006; Sonnentag et al., accepted for publication), to (ii) eliminate the additional effect of the microtopographic position of the LAI-2000 measurement for shrub LAI (Sonnentag et al., accepted for publication), and to (iii) minimize the potential field of view of the quantum sensor to roughly 0.9 times the average canopy height (with the inner three rings the sensor’s view limit is 43° and tangent (43°) is 0.9) to guarantee measurement independence along the transects.

Based on theoretical considerations and subsequent validation, Chen (1996) and Chen et al. (1997) introduced the fol-

lowing equation to derive tree LAI of boreal forest canopies from LAI_e :

$$LAI = (1-\alpha)LAI_e \frac{\gamma_E}{\Omega_E} \quad (1) \quad 251$$

where α is the woody-to-total leaf area ratio (to account for the contribution of woody canopy elements to light interception), LAI_e is the “effective” LAI [m^2/m^2], γ_E is the needle-to-shoot area ratio (to account for clumping within shoots), and Ω_E is the element clumping index (to account for clumping at spatial scales larger than shoots). Tree LAI for each flag of the tree transects was calculated from LAI_e using Eq. (1). A critical component in the application of Eq. (1) is the reliable estimation of γ_E , Ω_E , and especially α (Chen et al., 2006).

For the estimation of γ_E for tamarack, we followed the approach of Chen (1996). Since *Larix* sp. are a shade intolerant species (Olaczek, 1986), we took shoot samples from tamarack trees growing under two different growth conditions in terms of light availability. A total of 45 shoot samples were taken from trees of a central forest patch (referred to as forested bog): one dominant (D), one co-dominant (M), and one suppressed (S) tree, at three different height levels: top (T), middle (M), and bottom (L), resulting in nine classes with five shoot samples each: DT, DM, DL, MT, MM, ML, MS, ST, SM, and SL. To guarantee sampling consistency, the same sampling scheme according to tree height was applied to randomly selected, isolated trees (with one tree corresponding to the average height of each dominance category) located in an open area of the Mer Bleue bog (referred to as open bog), also resulting in a total of 45 shoot samples. All 90 shoot samples were stored in electrical coolers at a temperature of around 0° and analyzed in the laboratory within 3 days of sampling. Projected shoot areas for the simplified 3-angle projection method of Chen (1996) were measured using the apparatus described by Chen et al. (2006). The apparatus consists of a Toshiba PDR-4300 digital camera (Toshiba American Information Systems Inc., Irvine, CA, USA) mounted on a firm stand, a Prolite 5000 light box (Kaiser Fototechnik GmbH & Co. KG, Buchen, Baden-Wuerttemberg, Germany), and the WinSeedle (v2003a) image analysis software (Regent Instruments Inc., Quebec City, Quebec, Canada). A volume displacement method was used to measure the total needle area in a shoot (Chen et al., 1997). The conversion of the displaced volume to the surface area of tamarack needles was accomplished with an empirical equation for needles with elliptical cross sections according to the needle thickness-to-width ratio provided by Chen et al. (2006). For black spruce we used $\gamma_E = 1.36$ as estimated by Chen (1996).

For the quantification of clumping at spatial scales larger than shoots we used the Tracing Radiation and Architecture of Canopies (TRAC) instrument (3rd Wave Engineering, Napean, Ontario, Canada) based on a gap size distribution theory (Chen & Cihlar, 1995) to measure Ω_E directly in the field. The TRAC instrument was used five times each along mbt1 and mbt2 on sunny days during the last week of August 2005 to determine Ω_E for black spruce and tamarack separately.

The biggest source of uncertainty in the application of Eq. (1) is considered to be α . Ideally, its reliable estimation

303 requires destructive sampling (Chen et al., 2006). For black
 304 spruce we used $\alpha=0.15$ as provided by Chen et al. (2006). Due
 305 to the logistical constraints of harvesting a tree, we approxi-
 306 mated α for tamarack by taking the average of two estimates of
 307 α determined with two different methods. The first estimate of α
 308 was based on a set of tree morphological measurements in
 309 combination with intermediate results obtained from the
 310 estimation of γ_E for tamarack (Appendix A). The second
 311 estimate of α is based on seven growing and non-growing
 312 season (leaf-off) LAI-2000 measurements (Barr et al., 2004),
 313 taken at the same seven flags of mbt1.

314 Finally, tree LAI for each flag was calculated from LAI_c
 315 using Eq. (1) with γ_E , Ω_E , and α weighted according to basal
 316 area (data not shown) for black spruce and tamarack.

317 Shrub LAI for each flag of the tree and shrub transects was
 318 calculated from LAI_c with a simplified version of Eq. (1)
 319 following Sonnentag et al. (accepted for publication):

$$\text{LAI} = (1-\alpha)\text{LAI}_c \quad (2)$$

320 where α is the woody-to-total area ratio, weighted according
 321 to percent cover of each species at each flag (data not shown).
 322 Species-specific values for α for the shrub canopy of Mer
 324 Bleue bog are provided by Sonnentag et al. (accepted for
 325 publication).

326 2.3. Multiple endmember spectral mixture analysis

327 Mixture decomposition with SMA is a widely applied
 328 technique in passive optical remote sensing for determining
 329 fractions of pixel components. SMA has been successfully
 330 applied in a wide range of disciplines including forestry (e.g.,
 331 Roberts et al., 2004), geology (e.g., Bryant, 1996), social
 332 sciences (e.g., Schweik & Green, 1999), and urban studies (e.g.,
 333 Wu & Murray, 2003). In SMA it is assumed that the spectral
 334 reflectance of a pixel (ρ'_λ) is a mixture of the spectral reflectance
 335 of individual scene components (endmembers), each weighted
 336 according to their abundance to produce the mixture. Further-
 337 more, it is typically assumed that the mixture is linear and that
 338 multiple scattering is negligible resulting in minimal interaction
 339 between scene elements (Adams et al., 1993; Hall et al., 1995;
 340 Roberts et al., 1993). The model is described by:

$$\rho'_\lambda = \sum_{i=1}^N f_i \rho_{i\lambda} + \varepsilon_\lambda \quad (3)$$

342 where $\rho_{i\lambda}$ is the spectral reflectance of endmember i for a
 343 specific band (λ), f_i is the fraction of the endmember, N is the
 344 number of endmembers, and ε_λ is the residual error. A common
 345 way to assess the fit of an endmember model is by the root mean
 346 square error (RMSE), calculated as:

$$\text{RMSE} = \sqrt{\frac{\sum_{\lambda=1}^M (\varepsilon_\lambda)^2}{M}} \quad (4)$$

where M is the number of bands. To produce accurate fractions,
 two constraints have to be imposed on the mixture decompo-
 sition. The first constraint requires that the fractions sum up to
 one and the second constraint requires the fractions to be non-
 negative (Heinz & Chang, 2001).

One of the most critical steps in the application of mixture
 decomposition is the selection and proper spectral character-
 ization of suitable endmembers (Dennison & Roberts, 2003a;
 Tompkins et al., 1997). The spectral signature of endmembers
 can be determined by spectroradiometer measurements in the
 field or in the laboratory, selection of “pure” endmember pixels
 from the image to be unmixed, or simulation with a radiative
 transfer model. However, using a fixed set of endmembers, each
 with a single invariant spectral signature is a significant
 simplification of the real world and a fundamental limitation
 of SMA since it might result in poor accuracy of fractions
 (Petrou & Foschi, 1999; Song, 2005; Theseira et al., 2003).
 Furthermore, SMA uses the same number of endmembers for
 each pixel, not considering whether the respective endmember
 is present in a pixel or not. To overcome these two limitations of
 SMA, Roberts et al. (1998) introduced multiple endmember
 spectral mixture analysis (MESMA) to account for the spectral
 variability of endmembers and the varying number of end-
 members on a per-pixel basis. In MESMA, endmembers for
 mixture decomposition are selected from a site-specific spectral
 library containing the spectral signatures of suitable end-
 members. The endmember combination producing the lowest
 RMSE is assigned to each pixel (Roberts et al., 1998).

MESMA has been successfully applied in a wide range of
 remote sensing studies including snow cover and area mapping
 (e.g., Painter et al., 2003), plant species mapping (e.g., Dennison
 & Roberts, 2003a,b; Roberts et al., 1998, 2003), soil mapping in
 arid lands (e.g., Okin et al., 2001), landform mapping (e.g.,
 Ballantine et al., 2005), fire temperature mapping (e.g.,
 Dennison et al., 2006), urban morphology (e.g., Rashed et al.,
 2003), and planetary mapping (e.g., Johnson et al., 2006; Li &
 Mustard, 2003).

Based on field observations, the spectral similarity among
 tree and shrub canopies found in an exploratory study (data
 not shown), and aerial photographs, it was determined that a
 three endmember model consisting of a general sunlit vascular
 plant canopy, sunlit *Sphagnum* moss, and shadow would be

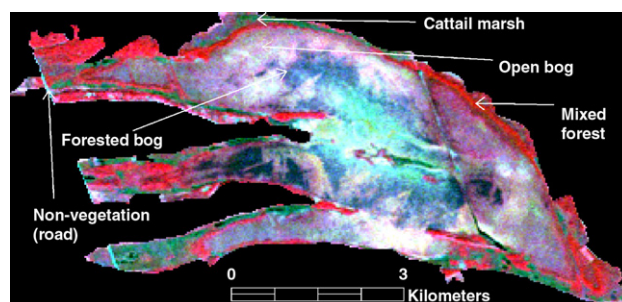


Fig. 3. False color composite (4, 3, 2 band combination) of the clipped subset of the Landsat TM scene of Mer Bleue, demonstrating the different spectral characteristics of the five considered land cover classes.

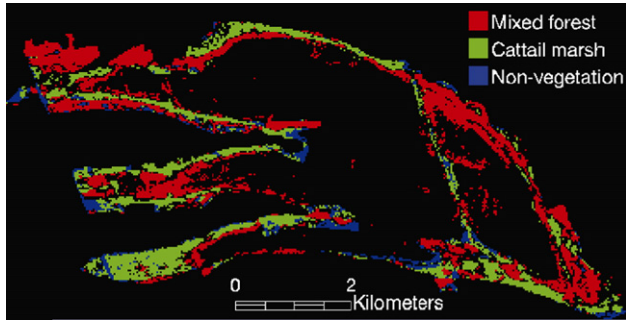


Fig. 4. Mixed forest, cattail marsh, and non-vegetation pixels excluded from the Mer Bleue subset with SAM to obtain the open and forested portions of Mer Bleue bog with pristine species composition and vertical vegetation structure for spectral unmixing.

390 suitable for Mer Bleue bog. The spectral characterization of
 391 the sunlit *Sphagnum* moss and shadow endmembers was
 392 accomplished with branch scale spectroradiometer measure-
 393 ments in the field (Section 2.4). The sunlit vascular plant
 394 canopy endmember was spectrally characterized using “pure”
 395 image pixels (Section 2.5). For both SMA and MESMA,
 396 fractions were constrained to sum to 1 and RMSE was re-
 397 stricted to ≤ 0.025 . Pixels exceeding this RMSE value were
 398 left unmodelled. No negative or superpositive abundance
 399 fractions were allowed for the sunlit vascular plant canopy
 400 and sunlit *Sphagnum* moss endmembers. No minimum abun-

dance fraction for the shadow endmember was set. Its maxi- 401
 mum abundance fraction was set to 0.80. 402

Mixture decomposition with SMA and MESMA on Landsat 403
 TM bands 1 through 5 was performed with VIPER Tools de- 404
 veloped at the Department of Geography at University of 405
 California Santa Barbara as an add-on for the ENVI software 406
 package (<http://www.vipertools.org>). 407

2.4. Spectral measurements 408

We measured the spectral reflectance of “pure” *Sphagnum* 409
 moss ground cover (for the spectral characterization of the sunlit 410
Sphagnum moss endmember), the shrub canopy with a 411
Sphagnum moss ground cover background (for the parameter- 412
 ization of the geometric-optical radiative transfer model in 413
 Section 2.6), and tree and shrub shadows at the branch scale (for 414
 the spectral characterization of the shadow endmember) be- 415
 tween 350 and 2500 nm at 2 nm sampling intervals in the field 416
 with a FieldSpec Pro spectroradiometer (Analytical Spectral 417
 Devices (ASD) Inc., Boulder, Colorado, USA) during the last 418
 week of August 2005. To capture the intra-canopy variability in 419
 spectral reflectance of shrubs and the inter-species as well as the 420
 intra-species variability in spectral reflectance of *Sphagnum* 421
 moss as influenced by different volumetric moss moisture con- 422
 tents and environmental conditions, we took several sets of 423
 spectral reflectance measurements at different locations with 424

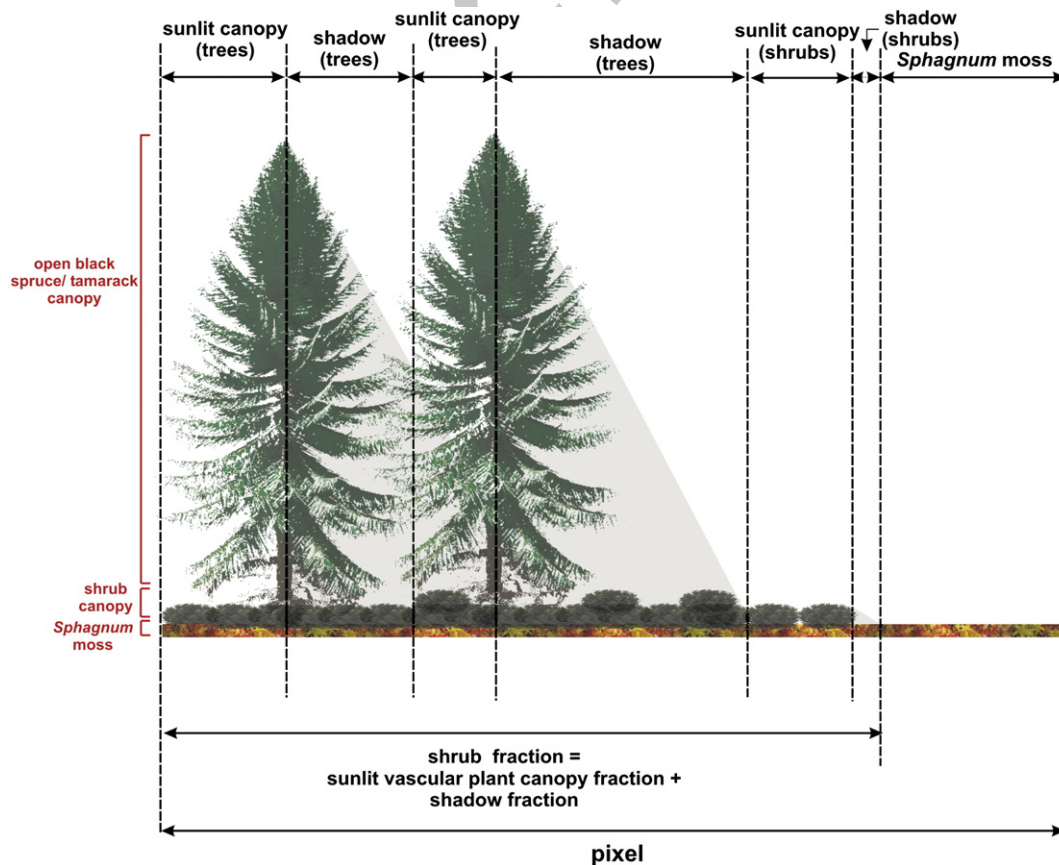


Fig. 5. Conceptualization of our shrub LAI mapping approach: the open tree canopy and its shadow are both “underlain” by shrub canopy, and thus the shrub fraction of a pixel is the sum of the sunlit vascular plant canopy and shadow fractions, i.e. $[1 - \text{sunlit } Sphagnum \text{ moss fraction}]$.

425 different shrub and *Sphagnum* moss species under different
 426 moisture conditions across the bog. Each set of spectral re-
 427 flectance measurements consisted of six individual measure-
 428 ments taken within a radius of 0.5 m. All spectral reflectance
 429 measurements were taken between 10 am and 2 pm at a height
 430 of about 0.25–0.30 m above the target (sensor field of view:
 431 25°), and were standardized to reflectance using a Spectralon
 432 diffuse reflectance target (Labsphere, North Sutton, New
 433 Hampshire, USA). The raw data of all spectral measurements
 434 acquired for this study are available from the corresponding
 435 author upon request.

436 2.5. Landsat TM image preprocessing

437 The Landsat TM scene at 30 m-resolution used in this study
 438 was acquired September 6, 2005. The scene was ordered as a
 439 radiometrically and geometrically corrected L1G product in
 440 UTM coordinates (North American Datum 1983). The digital
 441 numbers of the scene were transformed into radiance values
 442 at the top of the atmosphere by using the gains and offsets
 443 provided with the image. The atmospheric correction to convert
 444 the radiance values at the top of the atmosphere into spectral
 445 reflectance values at the ground surface was accomplished with
 446 the Second Simulation of Satellite Signal in the Solar Spectrum
 447 (6S) code (Vermote et al., 1997) using atmospheric conditions
 448 from Ottawa at the date of scene acquisition as input. The
 449 atmospheric water vapour and ozone burden data required by 6S
 450 were obtained from the Moderate Resolution Imaging Spectro-
 451 radiometer (MODIS) Atmospheric Profile data product ([http://](http://daac.gsfc.nasa.gov/MODIS/)
 452 daac.gsfc.nasa.gov/MODIS/). Atmospheric optical depth which
 453 is crucial in the derivation of spectral reflectance values at the
 454 ground surface from radiance values at the top of the atmo-
 455 sphere was simulated by 6S based on a standard continental
 456 aerosol profile using the meteorological parameter “visibility”
 457 as provided for Ottawa for the date of scene acquisition by
 458 Environment Canada (<http://climate.weatheroffice.ec.gc.ca>).
 459 All subsequent processing steps related to the calculation of
 460 SVI, SMA, and MESMA were performed on a subset of the
 461 Landsat TM scene, clipped to the boundary of Mer Bleue
 462 (Fig. 3). For our purposes of peatland LAI mapping we dis-
 463 tinguish between the five land cover classes “open bog”,
 464 “forested bog”, “mixed forest”, “cattail marsh”, and “non-veg-
 465 etation” (including open water and roads), all of which have
 466 significantly different spectral characteristics (Fig. 3).

467 To test the applicability of common SVI for peatland LAI
 468 mapping, we computed NDVI, SR, and RSR for OLS regression
 469 analysis with our tree and shrub LAI field measurements.

470 Our LAI mapping efforts with MESMA were aimed at the
 471 open and forested portions of Mer Bleue bog with pristine
 472 species composition and vertical vegetation structure (Fig. 3).
 473 Therefore, parts of Mer Bleue that are characterized by mixed
 474 forest, cattail marsh or non-vegetation were identified and ex-
 475 cluded prior to mixture decomposition using the Spectral Angle
 476 Mapper (SAM; Kruse et al., 1993), a supervised classification
 477 method (Fig. 4). The spectral characterization of the reference
 478 reflectance spectra for SAM and the sunlit vascular plant canopy
 479 endmember of our three-endmember model was accomplished

with the Minimum Noise Feature (MNF) transformation (Green 480
 et al., 1988) and the Pixel Purity Index (PPI; Boardman et al., 481
 1995) applied to MNF transformed data for the identification of 482
 spectrally “pure” pixels as implemented in the ENVI software 483
 package (ENVI, 2004). To guarantee that we obtain just the 484
 purest pixels for mixed forest, cattail marsh, non-vegetation, and 485
 the sunlit vascular plant canopy endmember, we applied the PPI 486
 approach successively, using different PPI thresholds for the 487
 four different classes. For SAM and spectral endmember 488
 characterization we averaged the 10 purest pixels of each class. 489

490 2.6. Tree and shrub LAI mapping

Inspired by the study of Hall et al. (1995), which empirically 491
 and theoretically demonstrates the relationship between shadow 492
 fraction and tree LAI, we investigated the nature of this 493
 relationship for the Mer Bleue bog using the geometric-optical 494
 radiative transfer model 4-Scale (Chen & Leblanc, 1997) and 495
 nonlinear OLS regression analysis. Our hyperspectral 4-Scale 496
 simulations were aimed to calculate shadow fractions for tree 497
 LAI values ranging from 0 to 3 for a spatial domain of the size 498
 of a Landsat TM pixel (900 m²). The calculation of domain 499
 fractions with 4-Scale requires information on the optical prop- 500
 erties of foliage and background in the form of hyperspectral 501
 leaf scale transmittance and reflectance spectra and hyperspec- 502
 tral branch scale reflectance spectra, respectively. To investigate 503
 the nature of the regression relationship between tree LAI and 504
 shadow fraction, we used the sum of shaded crown and shaded 505
 background as the total shadow fraction of our modelling do- 506
 main. Details on the major features of 4-Scale and information 507
 on its parameterization for this study is provided in Appendix B. 508

All tree and shrub transects were located on the Landsat TM 509
 scene. To estimate the average tree and shrub LAI for Landsat 510
 TM pixels along transects, all LAI-2000 field measurements 511
 taken within each transect pixel were averaged. In total, we 512
 obtained 17 pixels of the forested portions of Mer Bleue bog to 513
 which we were able to assign an average value of field-meas- 514
 ured tree LAI (LAI-2000 instrument). Depending on the rela- 515
 tive location of each transect on the Landsat TM scene, the 516
 number of field-measured tree LAI per pixel varied between one 517
 (for three pixels) and four (for one pixel), respectively. Average 518
 tree LAI of six and seven pixels was based on two and three 519
 field measurements, respectively. 520

Tree LAI of the forested portions of Mer Bleue bog was 521
 mapped through inversion of the equation describing the 522
 empirical relationship between shadow fraction obtained from 523
 mixture decomposition and tree LAI as determined through our 524
 simulations with 4-Scale. Tree LAI for the mixed forest pixels 525
 of Mer Bleue (Fig. 4) was mapped through inversion of the 526
 published exponential equation of the empirical relationship 527
 between RSR and mixed forest tree LAI provided by Chen et al. 528
 (2002): 529

$$529 \text{ RSR} = 9.3 - 9.3e^{(-\text{LAI}/2.93)}. \quad (5)$$

Regarding shrub LAI, we obtained 29 pixels in total, 15 530
 pixels corresponding to tree transects (two of the 17 pixels of 533

the forested portions close to a drainage ditch were neglected because the shrub canopy reached an average height of 1 m) and 14 pixels corresponding to shrub transects, to which we were able to assign an average value of field-measured shrub LAI (LAI-2000 instrument). The number of field-measured shrub LAI per pixel varied between one (for five pixels) and four (for two pixels), respectively. Average shrub LAI of 10 and 12 pixels was based on two and three field measurements, respectively. Shrub LAI was mapped through inversion of the empirical relationship between shrub fraction and field-measured shrub LAI. The assumption underlying this approach is the observation that the open tree canopy of Mer Bleue bog is “underlain” by shrub canopy, and the shadow produced by trees is also “underlain” by shrub canopy. Thus, the shrub fraction of a pixel is assumed to be the sum of the sunlit vascular plant canopy and shadow fractions, i.e. $[1 - \text{sunlit } Sphagnum \text{ moss fraction}]$ (Fig. 5). Both approaches to map tree and shrub LAI based on fractions obtained from SMA and MESMA were validated using “leave-one-out”-cross-validation (LOOC) (Isaaks & Srivastava, 1989).

Our approach to map shrub LAI based on shrub fraction is not applicable to shrubs under the mixed forest canopy due to the relatively high degree of crown closure. Therefore, shrub LAI for mixed forest pixels was set to a constant value of 2.50 (1.13), which is the average (S.D.) shrub LAI measured along transect mbt5. Due to the lack of field-measured LAI, cattail LAI was set to a constant maximum growing season value of 3.63 (M.-C. Bonneville, unpublished data).

3. Results and discussion

3.1. Field measurements

A summary of needle-to-shoot area ratios of tamarack growing at Mer Bleue bog under two different lighting conditions is provided in Table 2. To the best of our knowledge, there has been no study reporting estimates of γ_E for tamarack.

Table 2
Needle-to-shoot area ratios (γ_E) of tamarack at Mer Bleue bog, growing under two different growth conditions in terms of light availability

Sample	Open bog		Forested bog	
	Mean	S.D.	Mean	S.D.
DT	1.56	0.34	1.33	0.27
DM	0.97	0.32	1.57	0.22
DL	1.78	0.86	1.53	0.39
MT	1.70	0.45	1.41	0.51
MM	1.49	0.16	1.55	0.06
ML	1.21	0.32	1.50	0.30
ST	1.04	0.17	1.06	0.70
SM	1.35	0.35	1.73	0.74
SL	1.37	0.34	1.34	0.28
Mean	1.39	0.38	1.45	0.38

For each growth condition, 45 shoot samples were taken from three trees: one dominant (D), one co-dominant (M), and one suppressed (S) tree, at three different height levels: top (T), middle (M), and bottom (L), resulting in nine classes with five shoots samples each: DT, DM, DL, MT, MM, ML, MS, ST, SM, and SL.

Table 3
Mer Bleue bog-specific clumping indices (Ω_E) of black spruce and tamarack and woody-to-total area ratios (α) of tamarack for use in Eq. (1) to derive LAI from LAI_c after Chen et al. (1997)

Parameter	Method	Tree species	No. of samples	Min.	Max.	Mean
Ω_E	TRAC	Black spruce	4	0.77	0.96	0.87
Ω_E	TRAC	Tamarack	4	0.77	0.95	0.87
α	Morphological measurements	Tamarack	12	0.12	0.17	0.15
α	Leaf-off LAI-2000 measurements	Tamarack	7	0.19	0.37	0.30

Comparisons of Table 2 with published estimates of γ_E for several coniferous tree species in Canada show that the mean values for tamarack under both growth conditions are considerably smaller. Chen et al. (2006) reported γ_E estimates of 1.66, 1.61, 1.71, and 1.91 for a mature and young Douglas fir stand on Vancouver Island, a balsam fir stand in New Brunswick, and a white pine stand in southern Ontario, respectively. The variation of γ_E among the two different growth conditions and also among the nine classes of each growth condition does not show any pattern. This is in contrast to the systematic variation of γ_E observed for different coniferous tree species among the nine classes by Chen et al. (2006), with the highest values for γ_E in dominant trees, followed by co-dominant and suppressed trees, respectively. Within a tree they reported generally higher γ_E values for shoots at higher levels than for shoots at lower levels. Considering the harsh growth conditions in acidic and nutrient-poor ombrotrophic peatlands, our generally small γ_E estimates for tamarack compared to the values reported by Chen et al. (2006) and the lack of any systematic variation between different height levels within trees is consistent with their hypothesis that the needle-to-shoot area ratio is mainly determined by growth conditions. Furthermore, our uniform γ_E estimates reflect the openness of the tree canopy at Mer Bleue bog where inter-tree shading does not result in more favorable lighting conditions of more open areas when compared to denser tamarack stands (Gower & Richards, 1990). For the calculation of tree LAI from LAI_c using Eq. (1) after Chen et al. (1997) we used the average γ_E value between open and forested bog of 1.42 (Table 2).

Our Mer Bleue bog-specific mean Ω_E estimate for black spruce of 0.87 is in reasonable agreement with the values provided by Chen et al. (2006) for the same species at two forest sites in Canada. Similar to the needle-to-shoot area ratio for tamarack reported above, there has been no study reporting Ω_E and α estimates for tamarack (Table 3). Our mean Ω_E estimate for tamarack is the same as for black spruce, i.e. reflecting a relatively high degree of foliage clumping.

The quick and reliable non-destructive estimation of α is still in its infancy, and often best estimates for this parameter are used in Eq. (1) (Chen et al., 2006). To reduce the considerable amount of uncertainty introduced by applying best estimates, we determined α with two simple non-destructive methods providing contrasting results (Table 3). Our α estimate of 0.15 based on morphological measurements is in the lower range compared to α

t4.1 Table 4
t4.2 Summary of field-measured tree and shrub LAI summarized according to the
t4.3 relative location of each transect on the subset of Landsat TM scene

t4.3		Tree LAI [m ² /m ²]	Shrub LAI (forested bog) [m ² /m ²]	Shrub LAI (open bog) [m ² /m ²]
t4.4	No. of pixels	17	15	14
t4.5	Min. LAI	0.23	0.76	0.73
t4.6	Max. LAI	3.06	2.87	3.05
t4.7	Mean LAI	1.59	1.57	1.50
t4.8	S.D.	0.83	0.61	0.67

612 estimates reported by Chen et al. (2006) for other coniferous tree
613 species in Canada, whereas an α estimate of 0.30 is in the higher
614 range. We assume that the α estimate based on morphological
615 measurements is underestimated due to the nature of the approach
616 of simply using mean values of a few morphological measure-
617 ments. Our α estimate based on leaf-off LAI-2000 measurements
618 is most likely overestimated due to the timing of the non-growing
619 season LAI-2000 measurement at dusk after a sunny day in mid-
620 November. The short sunset provided us just with a very short
621 time window with diffuse light conditions to take the measure-
622 ments. The highest individual α values coincide with the last
623 measurements when it was probably too dark, resulting in an
624 overestimation of non-growing season LAI_c and thus α . We
625 assume that our two contrasting α estimates define the limits of its
626 actual mean value, and thus we used the average of both estimates
627 of 0.225 for application in Eq. (1).

628 The final averaged tree and shrub LAI values pixel after
629 correcting LAI_c for γ_E , Ω_E , and α (tree LAI) and for α (shrub
630 LAI) with Eqs. (1) and (2), respectively, are provided in Table 4.
631 Tree LAI varies over a wide range from 0.23 and 3.06, resulting
632 in a mean value of 1.59. This average tree LAI is much smaller
633 than the average tree LAI of several forest sites in Canada (Chen
634 et al., 2006), and thus reflects the low productivity of acidic and
635 nutrient-poor ombrotrophic peatlands. Shrub LAI varies over a
636 range similar to tree LAI, with a slightly lower mean shrub LAI
637 measured along transects located in open areas of the bog
638 compared to forested portions. The similar ranges and means of
639 tree and shrub LAI, respectively, provided by Table 4 indicate
640 the importance of the shrub canopy in the Mer Bleue bog's
641 hydrological and ecological functioning as described in several
642 studies (e.g., Lafleur et al., 2005; Moore et al., 2002).

643 3.2. Spectral vegetation indices for Mer Bleue

644 All three SVI computed from the atmospherically corrected
645 Landsat TM subset of Fig. 3 respond to the dense tree canopy
646 along drainage ditches and the beaver ponds with the highest
647 values for Mer Bleue (Fig. 6). Non-vegetation pixels yield the
648 lowest values for the respective SVI (e.g., the southern beaver
649 pond of the northern finger delineating Mer Bleue bog,
650 portions of the drainage dissecting the eastern half of Mer
651 Bleue bog). Intermediate between these two extremes are the
652 cattail marshes and areas of Mer Bleue bog characterized by
653 pristine species composition and vertical vegetation structure.
654 The central part of Mer Bleue bog, in particular, responds with
655 values for the respective SVI similar to non-vegetation pixels,

656 thus indicating sparse vascular vegetation. However, from
657 field observations and aerial photographs (data not shown) we
658 know that these central areas comprise very open patches of
659 typical black spruce and tamarack canopies over an also
660 relatively open and low shrub canopy. Thus, in these areas, the
661 major contributor to background reflectance is the *Sphagnum*
662 moss ground cover, with spectral features that do not allow for
663 the adequate characterization of the absorption in the red
664 portion of the visible range and the high reflectance of the
665 NIR range of the vascular plants (Fig. 8).

666 The linear OLS regression relationships between the SVI
667 of Fig. 6 and the field-measured tree and shrub LAI (open
668 bog) of Table 4 are provided by Fig. 7. Regarding tree LAI,
669 the highest value for R^2 is obtained for RSR ($R^2=0.27$),
670 followed by SR ($R^2=0.13$) and NDVI ($R^2=0.09$), respective-
671 ly. Generally, the R^2 values for the Mer Bleue bog are
672 significantly smaller than those obtained in boreal forest
673 ecosystems (e.g., Brown et al., 2000; Chen et al., 2002),
674 indicating for each pixel that there is no single SVI vs. tree
675 LAI linear regression relationship but a set of relationships, all
676 of which are a function of crown closure and thus of the nature

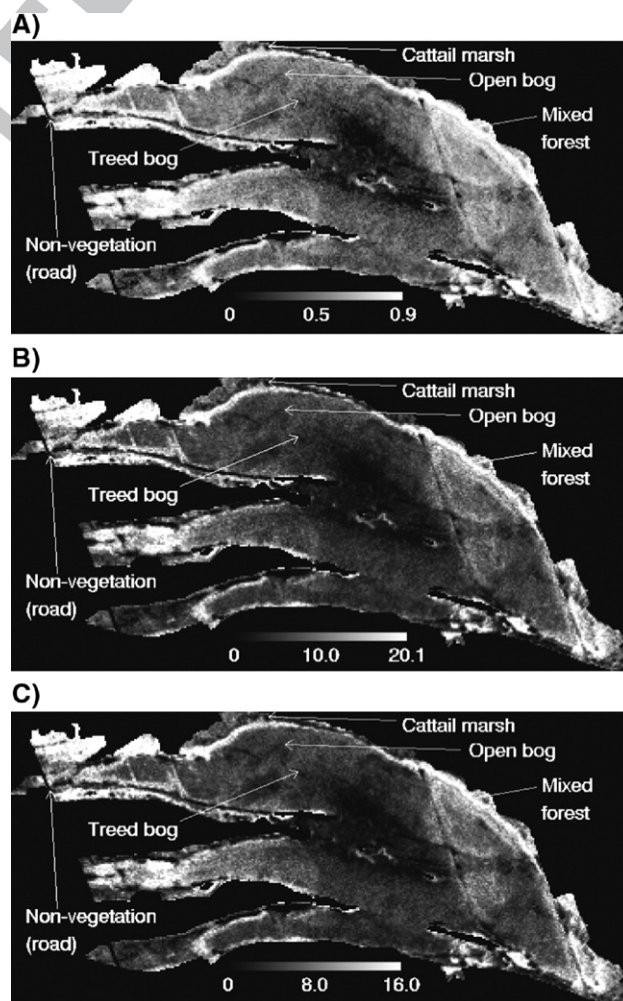


Fig. 6. Mapped SVI for Mer Bleue computed from the atmospherically corrected Landsat TM subset: (A) NDVI, (B) SR, and (C) RSR.

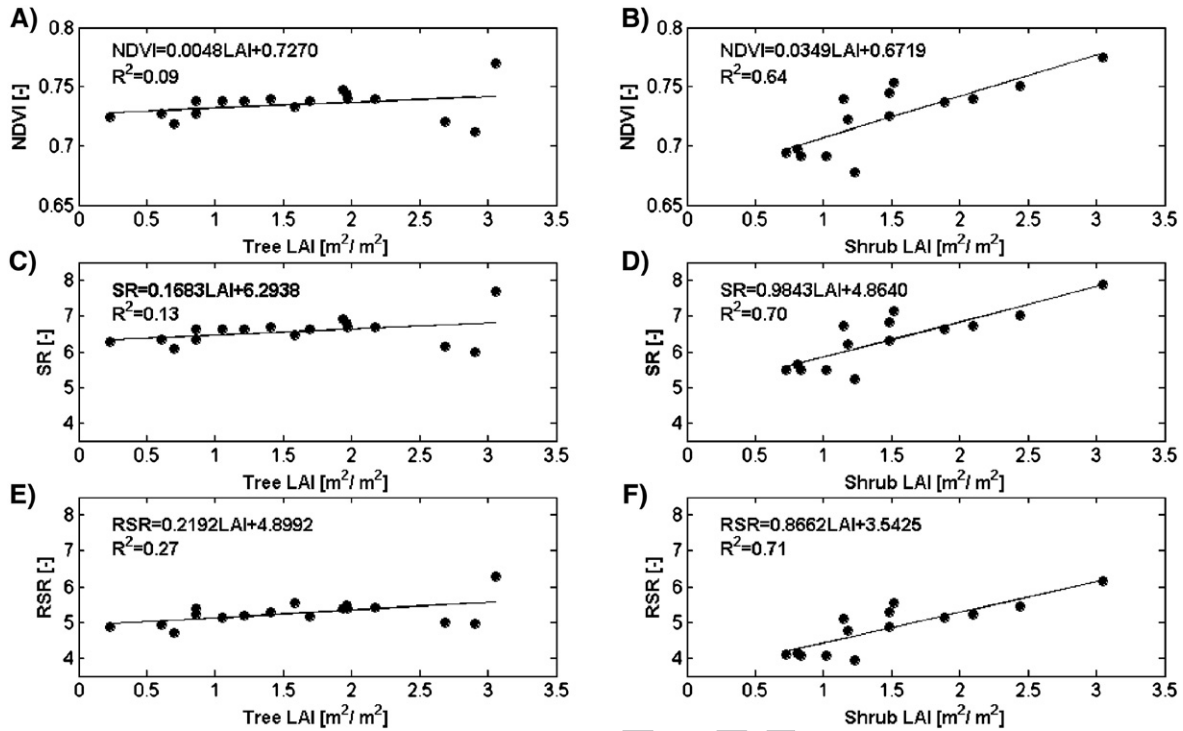


Fig. 7. Linear OLS regression relationships between SVI (Fig. 6) and field-measured tree and shrub LAI: A) NDVI vs. tree LAI, B) NDVI vs. shrub LAI, C) SR vs. tree LAI, D) SR vs. shrub LAI, E) RSR vs. tree LAI, and F) RSR vs. tree LAI.

677 of background reflectance. However, the general superiority
 678 of RSR over SR and NDVI for tree LAI mapping in boreal
 679 forests due to its capability to compensate for differences in
 680 canopy closure and background reflectance was demonstrated
 681 in several previous studies (e.g., Brown et al., 2000; Chen
 682 et al., 2002). For shrub LAI, the highest value for R^2 is again
 683 obtained for RSR ($R^2=0.71$), followed by SR ($R^2=0.70$) and
 684 NDVI ($R^2=0.64$), respectively. These significantly higher R^2
 685 values for all three SVI demonstrate their general applicability

to the shrub canopy of the open portions of the Mer Bleue bog. However, none of the SVI of Fig. 7 allows for mapping of shrub LAI of the forested portions of Mer Bleue bog.

3.3. Mixture decomposition with SMA and MESMA

We used nine *Sphagnum* moss reflectance spectra measured at Mer Bleue bog convolved to the wavelength range corresponding to the Landsat TM bands 1 through 5 for mixture

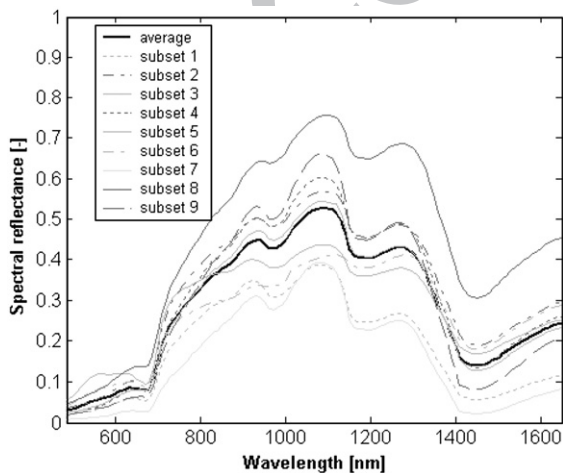


Fig. 8. *Sphagnum* moss reflectance spectra measured at Mer Bleue bog: nine individual sample sets for mixture decomposition with MESMA, and their average (bold line) for mixture decomposition with SMA.

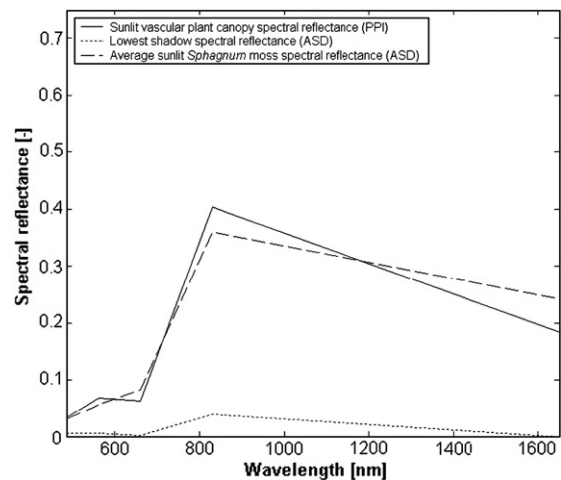


Fig. 9. Spectral characterization of the three-endmember model for mixture decomposition with SMA (convolved to the mid-points of the Landsat bands 1 through 5): sunlit vascular plant canopy, sunlit *Sphagnum* moss, and shadow.

693 decomposition (Fig. 8). All nine reflectance spectra are char-
 694 characterized by diagnostic reflectance differences in the visible,
 695 NIR, and SWIR distinguishing them from the reflectance spec-
 696 tra of vascular plants. Generally, *Sphagnum* moss is more refle-
 697 ctive in the red portion of the visible range and less reflective
 698 in the NIR range than vascular plants. Further characteristic
 699 features of *Sphagnum* moss reflectance spectra described by
 700 Bubier et al. (1997) are the strong water absorption features at
 701 about 980 and 1200 nm, resulting in three distinctive spectral
 702 reflectance peaks at about 930, 1100, and 1300 nm (Fig. 8).

703 However, the amplitudes of this general behavior varies over a
 704 wide range since it is significantly controlled by the near-
 705 surface volumetric moss moisture content, soil and water chem-
 706 istry, and environmental conditions such as light availability
 707 (Bryant & Baird, 2003; Bubier et al., 1997; Harris et al., 2005,
 708 2006).

709 We used the average of the nine *Sphagnum* moss reflectance
 710 spectra of Fig. 8 to spectrally characterize the sunlit *Sphagnum*
 711 moss endmember of our three-endmember model for SMA. For
 712 the spectral characterization of the shadow endmember, we

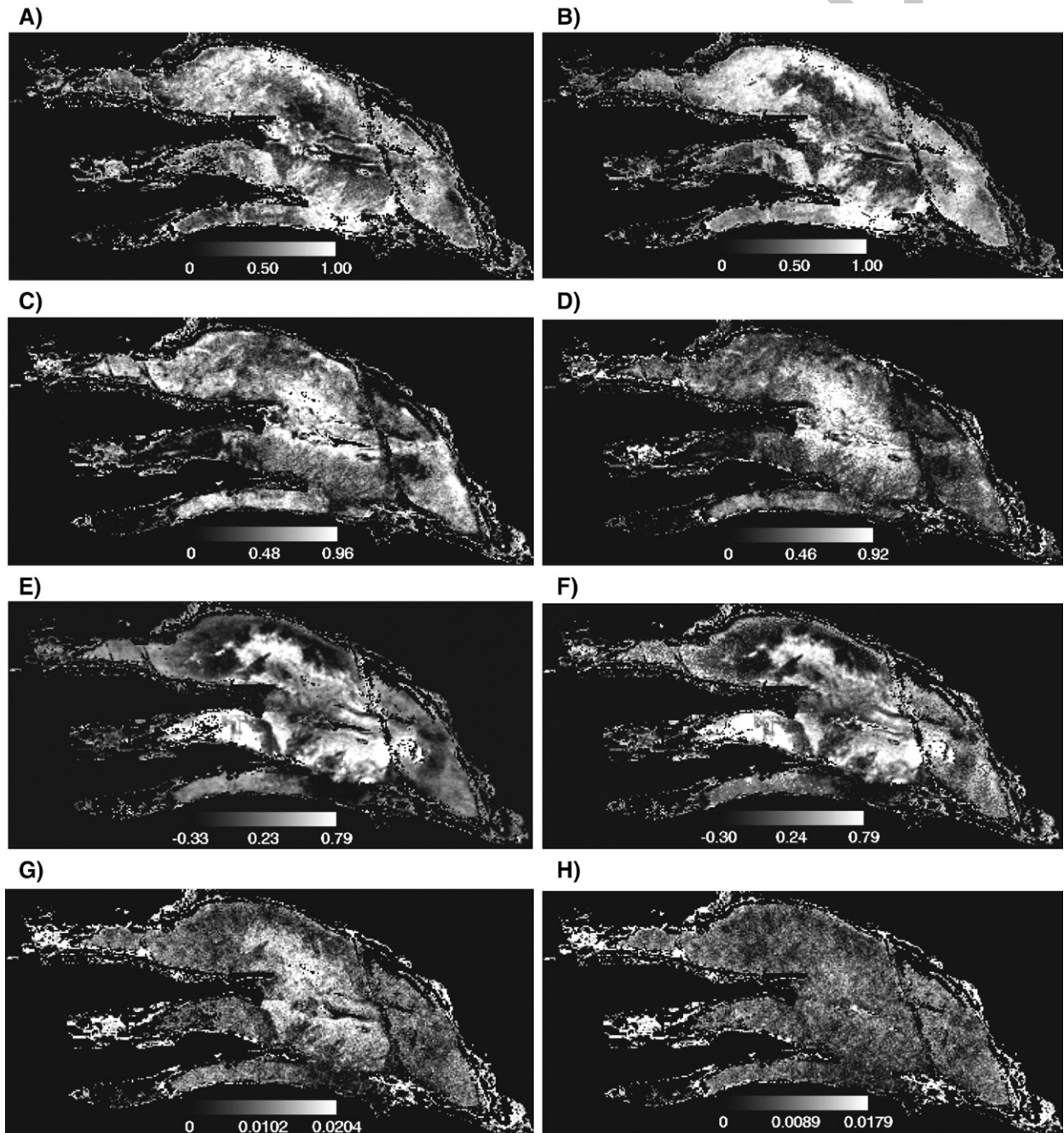


Fig. 10. Fractions and assessment of model fit for SMA and MESMA: A) sunlit vascular plant endmember (SMA), B) sunlit vascular plant endmember (MESMA), C) sunlit *Sphagnum* moss endmember (SMA), D) sunlit *Sphagnum* moss endmember (MESMA), E) shadow endmember (SMA), F) shadow endmember (MESMA), G) RMSE (SMA), and H) RMSE (MESMA).

Table 5			
Direct comparison of the classified Mer Bleue subsets obtained with SMA and MESMA (subset of Fig. 8)			
t5.3	Mer Bleue # pixels	29,734	
t5.4	Non-pristine (Fig. 4) # pixel	9856	
t5.5	Mer Bleue bog # pixels (%)	19,878 (100)	
		SMA	
		MESMA	
t5.7	Average reflectance spectra # pixels (%)	19,393 (97.56)	–
t5.8	Classified # pixels (%) ss 1	–	19 (0.10)
t5.9	Classified # pixels (%) ss 2	–	172 (0.87)
t5.10	Classified # pixels (%) ss 3	–	3720 (18.71)
t5.11	Classified # pixels (%) ss 4	–	1439 (7.24)
t5.12	Classified # pixels (%) ss 5	–	8 (0.04)
t5.13	Classified # pixels (%) ss 6	–	9104 (45.80)
t5.14	Classified # pixels (%) ss 8	–	5119 (25.75)
t5.15	Classified # pixels (%) ss 9	–	130 (0.65)
t5.16	Total # pixels (%)	19,393 (97.56)	19,711(99.16)

713 manually selected the field-measured shadow reflectance
714 spectrum with the lowest spectral reflectance values in the
715 visible, NIR, and SWIR ranges. The sunlit vascular plant
716 canopy endmember was spectrally characterized through the
717 combined use of MNF and PPI. The resulting sunlit vascular
718 plant canopy reflectance spectrum is similar to the sunlit
719 *Sphagnum* moss reflectance spectrum, indicating the influence
720 of the underlying *Sphagnum* moss ground cover on the overall
721 spectral response of the shrub canopy (Fig. 9).

722 For MESMA we built a spectral library that consisted of all
723 nine *Sphagnum* moss reflectance spectra (Fig. 8) together with
724 the sunlit vascular plant canopy and shadow endmembers
725 (Fig. 9) resulting in nine different three-endmember models.

726 The fractions of the three endmembers and the RMSE
727 obtained from mixture decomposition with SMA and MESMA,
728 respectively, are provided in Fig. 10. For both mixture decom-
729 position approaches, the distributions of the sunlit vascular plant
730 canopy endmember are relatively uniform (Fig. 10A and B,
731 respectively). The highest sunlit vascular plant canopy fractions
732 are south of the northern margin and north of the southern
733 margin of Mer Bleue bog corresponding to open bogs where
734 trees are absent (Fig. 3). The lowest values occur in the central,
735 forested portions of Mer Bleue bog. This portion of the bog also
736 shows the lowest response to the SVI (Fig. 6), indicating sparse
737 vascular vegetation.

738 The spatial distributions of the sunlit *Sphagnum* moss
739 endmember (Fig. 10C and D, respectively) are the inverse of the
740 sunlit vascular plant canopy endmember, i.e. relatively uniform
741 except for the central portions, where the highest fractions
742 occur. High sunlit *Sphagnum* moss fractions are indicative of
743 the absence or a low density of the shrub canopy. The shadow
744 fractions from SMA and MESMA both show a clear pattern
745 corresponding to open and forested portions of the Mer Bleue
746 bog (Fig. 10E and F, respectively): areas where trees are absent
747 or that just contain individual, isolated trees are characterized by
748 the lowest shadow fractions, whereas forested portions are
749 characterized by the highest shadow fractions. Seventy pixels in
750 Fig. 10E and 66 pixels in Fig. 10F have unrealistic negative
751 shadow fractions, some of which occur in both images. How-
752 ever, since these pixels were all located in areas of Mer Bleue

753 that clearly correspond to cattail marsh, mixed forest, or non-
754 vegetation they were excluded from the subsequent analysis.
755 Most likely these pixels were simply misclassified by SAM.

756 Regarding the spatial distributions of RMSE, for both SMA
757 and MESMA the highest values occur in areas of Mer Bleue that
758 correspond to cattail marsh, mixed forest, or non-vegetation
759 (Fig. 10G and H, respectively), and thus were most likely also
760 misclassified by SAM. However, since these pixels have re-
761 alistic fractions, they were kept for the subsequent analysis.
762 Within the Mer Bleue bog, RMSE obtained from SMA covers a
763 wider range and shows more spatial variation than RMSE
764 obtained from MESMA. The highest RMSE values from SMA
765 occur in the central areas of the bog, which also show the
766 highest sunlit *Sphagnum* moss and shadow fractions.

767 The direct comparison of the classified Mer Bleue subsets
768 obtained with SMA and MESMA is summarized in Table 5. SMA
769 using the average *Sphagnum* moss reflectance spectra of Fig. 8
770 can be used to model the spectral response of 97.56% of the pixels
771 of the Mer Bleue subset, whereas MESMA using all nine
772 *Sphagnum* moss reflectance spectra successfully models 99.16%.

773 The spatial variation of the different *Sphagnum* moss reflec-
774 tance spectra of Fig. 8 used by MESMA shows that different
775 areas of the Mer Bleue bog are modeled best by different three-
776 endmember models (Fig. 11). For example, the spectral re-
777 sponse of forested central portions of the bog is modeled best
778 with a three-endmember model that includes subset 8 in Fig. 8,
779 whereas the open portions of the bog are modeled best with a
780 three end-member model that includes subset 6. Other subsets in
781 Fig. 8 such as subsets 1, 2, and 9 are of minor importance, the
782 three-endmember model that includes subset 7 is not used at all
783 (Table 5).

784 Qualitatively, the spatial distributions of all three end-
785 members in Fig. 10 obtained from SMA and MESMA, re-
786 spective, are good approximations of the spatially varying
787 pristine species composition and vertical vegetation structure
788 of Mer Bleue bog, thus indicating the general applicability
789 of our three end-member model to ombrotrophic peatlands.
790 However, the spatial variability and the greater range of RMSE
791 obtained from SMA compared to MESMA, and the lower
792 percentage of classified pixels indicate that the widely varying
793 spectral characteristics of the sunlit *Sphagnum* moss end-
794 member are not adequately described by the average *Sphag-*
795 *num* moss reflectance spectrum of Fig. 8, which might result in

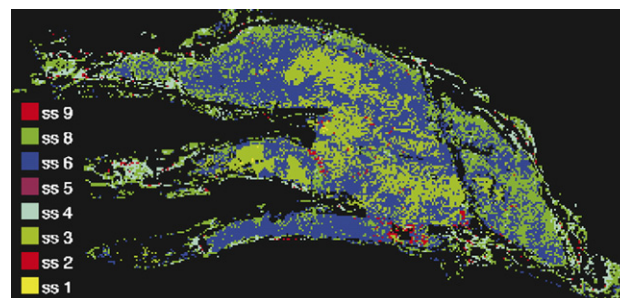


Fig. 11. Classified Mer Bleue subset (MESMA) using the nine reflectance spectra in Fig. 8 to describe the sunlit *Sphagnum* moss endmember (ss=subset of Fig. 8).

796 less accurate fractions. Furthermore, by using a range of dif-
 797 ferent *Sphagnum* moss reflectance spectra, the influence of the
 798 similarity between the average sunlit *Sphagnum* moss and the
 799 sunlit vascular plant canopy reflectance spectra is minimized
 800 (Fig. 9). Less accurate fractions limit the use of SMA for
 801 peatland LAI mapping as demonstrated in Section 3.5.

802 3.4. Geometric-optical radiative transfer modeling

803 The simulated relationship between shadow fraction and tree
 804 LAI is clearly not linear but appears to be of exponential nature
 805 and is best described with a nonlinear exponential equation of
 806 the general form (Fig. 12):

$$y = a - b \cdot \exp(-x/c) \quad (6)$$

808 where x and y are tree LAI and shadow fractions, respectively,
 809 and a , b , and c are regression constants. The constants a , b , and
 810 c of Eq. (6) describe the simulated exponential relationship
 811 between tree LAI and shadow fraction and were determined
 812 through unconstrained, non-linear OLS regression analysis as
 813 0.361, 0.326, and 1.698, respectively (Fig. 12).

814 The first constant in Eq. (6), a , is the maximum shadow
 815 fraction, and the second constant, b , is the difference between
 816 maximum shadow fraction and background shadow, i.e. shadow
 817 produced by the shrub canopy, since no trees are present at a tree
 LAI value of zero. Thus, for our simulated relationship the
 819 amount of shadow produced by the shrub canopy is estimated as
 820 0.035.

821 3.5. Tree and shrub LAI mapping using MESMA

822 Based on Eq. (6) we determined the regression relationships
 823 between tree LAI (Table 4) and shadow fractions obtained from
 824 SMA (Fig. 10E) and MESMA (Fig. 10F), respectively, through
 825 partially constrained non-linear OLS regression analysis
 826 (Fig. 13A and B, respectively). In both the regression relation-
 827 ships of Fig. 13A and B the first regression constant, a , was

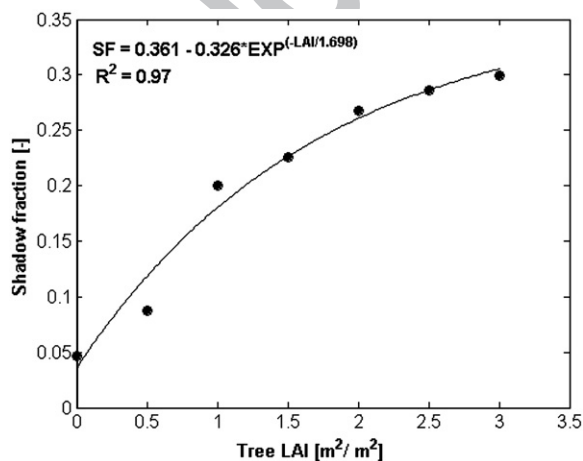


Fig. 12. Simulated exponential relationship between shadow fraction (SF) and tree LAI for a Landsat TM pixel of Mer Bleue bog.

828 preset to the maximum shadow fraction obtained from mixture
 829 decomposition (Fig. 10E and F, respectively). The second re-
 830 gression constant, b , was pre-set to the difference of the first
 831 regression constant and background shadow. An average back-
 832 ground shadow of 0.09 produced by the shrub canopy was
 833 calculated based on pixels corresponding to the three shrub
 834 transects mbs1, mbs2, and mbs3 located in open areas of the Mer
 835 Bleue bog where trees were absent. The third regression con-
 836 stant, c , was determined iteratively through the regression anal-
 837 ysis. Comparison of the R^2 values obtained through the mixture
 838 decomposition-based non-linear OLS regression (Fig. 13A and
 839 B, respectively) with those from the SVI-based linear OLS
 840 regression (Fig. 7A, C, and E, respectively) reveals that the
 841 shadow fraction is generally a strong predictor of tree LAI in
 842 ombrotrophic peatlands, with MESMA being superior over
 843 SMA as indicated by R^2 values of 0.75 (Fig. 13B) and 0.61
 844 (Fig. 13A), respectively. Similar findings demonstrating the
 845 general superiority of the shadow fraction over SVI for tree LAI
 846 estimation were made by Hall et al. (1995) and Hall et al. (2003).

847 For the estimation of shrub LAI based on shrub fraction we
 848 also applied the approach of partially constrained non-linear
 849 OLS regression analysis using Eq. (6) (Fig. 13C and D, re-
 850 spectively). A simple plot of field-measured shrub LAI and the
 851 shrub fractions obtained from SMA and MESMA revealed that
 852 the shrub fraction reaches a plateau at about 0.90 despite
 853 increasing shrub LAI. A possible reason for this might be that
 854 increasing shrub LAI is inherent with increasing shrub fraction
 855 up to a certain point, after which shrub LAI increases as a
 856 function of shrub height resulting in more foliage seen by the
 857 LAI-2000 instrument sensor but not necessarily in a higher
 858 fraction of shrubs covering the ground as determined through
 859 SMA and MESMA, respectively. This interpretation is sup-
 860 ported by the observation that the highest shrub LAI values
 861 along our transects were measured at mbt5 and mbs3, both of
 862 which are close to a drainage ditch and to the margin of Mer
 863 Bleue bog, respectively. Both areas are characterized by lower
 864 water table positions with more favorable growth conditions,
 865 resulting in higher and denser shrub canopies. In both OLS
 866 regression relationships of Fig. 13C and D, respectively, the first
 867 regression constant, a , was pre-set to a maximum shrub fraction
 868 of 0.90, representing the plateau of the exponential relationship.
 869 The background was set to zero, since if shrubs are absent,
 870 shrub LAI is supposed to equal zero. Our simple approach of
 871 calculating the shrub fraction as the sum of the sunlit vascular
 872 plant canopy and the shadow fraction (i.e. $[1 - \text{sunlit } Sphagnum$
 873 moss fraction]) most likely resulted in overestimation of the
 874 shrub fraction for some areas of Mer Bleue bog since it does not
 875 account for the situation where shadows produced by trees are
 876 “underlain” directly by *Sphagnum* moss, i.e. where the shrub
 877 canopy is absent. However, we assume that this overestimation
 878 is on average balanced by the underestimation that would result
 879 from the correction of 0.09 to the shadow fraction for the
 880 average shadow produced by the shrub canopy estimated above.
 881 Simple comparison of the R^2 values obtained through the mix-
 882 ture decomposition-based non-linear OLS regression (Fig. 13C
 883 and D, respectively) with those from the SVI-based linear OLS
 884 regression (Fig. 7B, D, and F, respectively) might suggest that

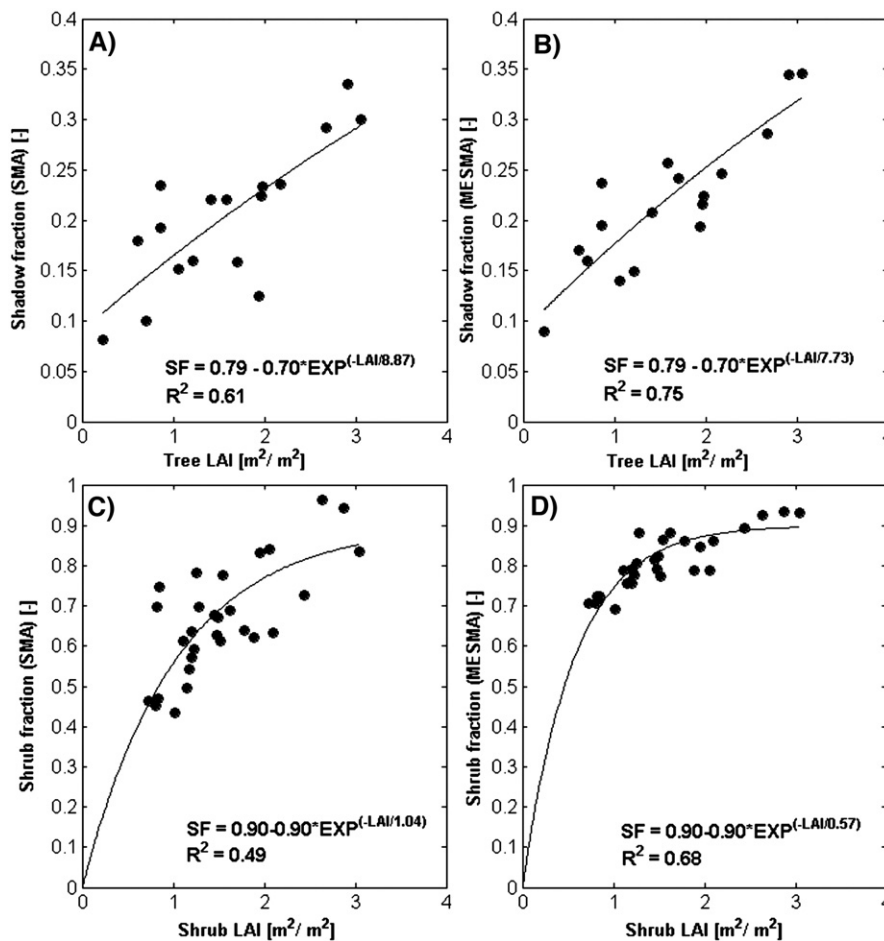


Fig. 13. Exponential relationships between shadow fractions derived from SMA and MESMA, respectively, and field-measured tree LAI based on Eq. (10), and between shrub fractions derived from SMA and MESMA, respectively, and field-measured shrub LAI, also based on Eq. (10).

885 the three SVI are generally stronger predictors of shrub LAI
 886 than the shrub fraction. However, SVI-based shrub LAI map-
 887 ping produces good results in open portions of the Mer Bleue
 888 bog but fails in its forested portions since these SVI respond to
 889 both shrub and tree canopies due to the low degree of canopy
 890 closure. Our approach based on shrub fraction is not sensitive to
 891 canopy closure, thus allowing for shrub LAI mapping in Mer
 892 Bleue bog's open and forested portions, and still produces
 893 acceptable results (Fig. 13C and D, respectively). Similar to tree
 894 LAI, MESMA is again superior over SMA as indicated by R^2
 895 values of 0.68 (Fig. 13D) and 0.49 (Fig. 13C), respectively.

896 3.6. Cross-validation

897 To gain confidence in our approaches we tested the tree and
 898 shrub LAI predictors derived from the shadow (Fig. 13A and B,
 899 respectively) and shrub fractions (Fig. 13C and D, respectively)
 900 with LOOC for the pixels of the tree and shrub transects. For
 901 tree LAI, as expected, the shadow fraction from MESMA
 902 (Fig. 14B) results in more accurate tree LAI estimates with R^2
 903 and RMSE values of 0.74 and 0.48, respectively, compared to
 904 tree LAI estimates based on SMA (Fig. 14A) with R^2 and
 905 RMSE values of 0.60 and 0.62, respectively. For both SMA and

MESMA, the slope and intercept are not significantly different
 from 1 and 0 (significance level=0.05), respectively.

Similar to tree LAI estimates, shrub LAI estimates based on
 the shrub fraction from MESMA (Fig. 14D) with R^2 and RMSE
 values of 0.68 and 0.42, respectively, are more accurate than
 shrub LAI estimates based on the shrub fraction from SMA
 (Fig. 14C) with R^2 and RMSE values of 0.55 and 0.73,
 respectively. The shrub LAI predictor based on shrub fraction
 obtained from SMA tends to overestimate shrub LAI in the
 higher range even though slope and intercept are not signifi-
 cantly different from 1 and 0 (significance level=0.05),
 respectively. Shrub LAI estimates based on MESMA are slight-
 ly underestimated at higher shrub LAI values and slightly
 overestimated at lower shrub LAI values with the slope just
 slightly different from 1 ($p=0.0417$) and the intercept not sig-
 nificantly different from 0 (significance level=0.05).

For the final production of the tree and shrub LAI maps for
 Mer Bleue based on inversion of Eq. (6), the shadow and sunlit
Sphagnum moss (i.e. [1 - sunlit *Sphagnum* moss]) fractions
 determined with MESMA were used (Fig. 15A–C). For the tree
 LAI calculation of the mixed forest pixels (Fig. 4) with Eq. (5)
 we constrained the RSR values of Fig. 6C to a maximum value
 of 9.2 (i.e. 29.47% of the mixed forest pixels). For the shrub

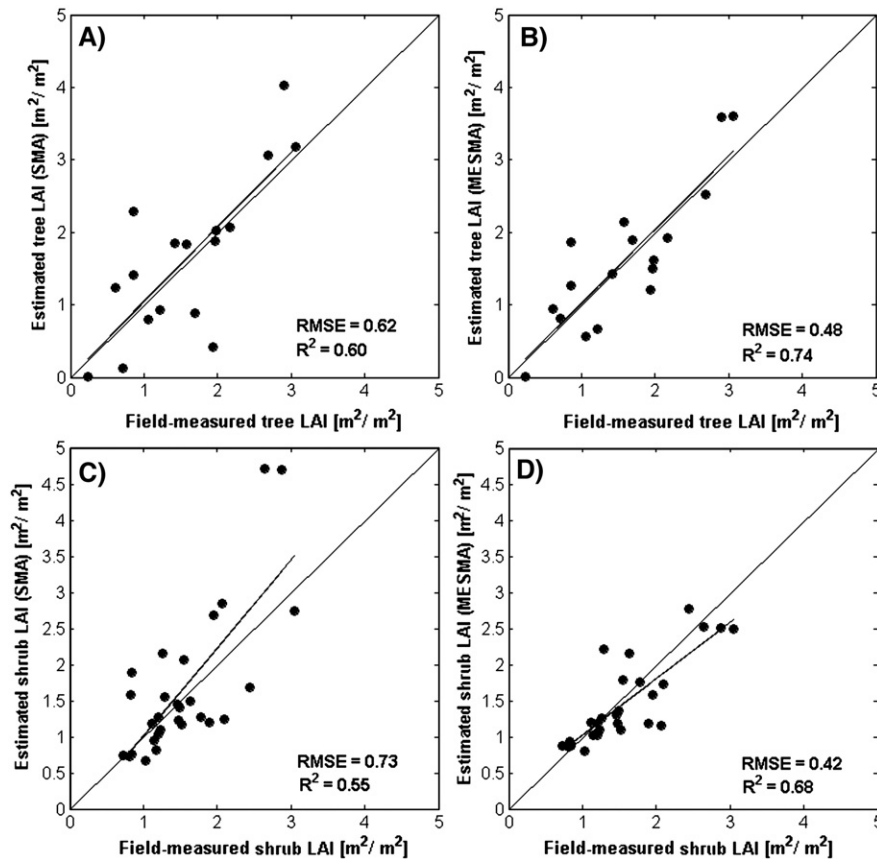


Fig. 14. “Leave-one-out”-cross-validation (LOOC) for tree LAI estimated based on shadow fraction obtained from SMA (A) and MESMA (B), and for shrub LAI estimated based on shrub fraction obtained from SMA (C) and MESMA (D).

929 LAI calculation with Eq. (6) based on Fig. 10F, we constrained
 930 the shrub fraction of a pixel to a maximum value of 0.89 (i.e.
 931 9.34% of Mer Bleue bog). We consider this constraint to be
 932 reasonable since at Mer Bleue bog a shrub fraction greater than
 933 0.90 over an area of 900 m² is unrealistic due to the bog’s
 934 microtopography. On average, hollows, which make up approx-
 935 imately one third of Mer Bleue bog’s surface area (Lafleur et al.,
 936 2005), have a percent cover of less than 0.5, and thus full shrub
 937 coverage over large areas does not exist (Sonnentag et al.,
 938 accepted for publication).

939 Total LAI was calculated as the sum of tree and shrub LAI
 940 (Fig. 15C). In all three maps, non-vegetation pixels (Fig. 4),
 941 pixels that were excluded due to negative shadow fractions
 942 (Fig. 10F), and unclassified pixels (Fig. 11) were set to NoData.
 943 Qualitatively, the LAI maps of Fig. 15 capture the spatial
 944 variation of the species composition and vertical vegetation
 945 structure of Mer Bleue quite well when compared to Fig. 3. As
 946 expected, the highest total LAI values occur along beaver ponds
 947 and drainage ditches, whereas the Mer Bleue bog is character-
 948 ized by considerably lower total LAI values. A striking feature
 949 of the shrub LAI map is the generally low shrub LAI values in
 950 the central forested parts of Mer Bleue bog as indicated by the
 951 fractions of Fig. 10 (Fig. 15B). The SVI of Fig. 6 indicate sparse
 952 vascular vegetation for these portions of the Mer Bleue bog,
 953 which would result in low total LAI values. However, the total
 954 LAI of these areas is in the same range as for the open portions

of Mer Bleue bog, with the tree LAI as the major contributor to
 total LAI.

4. Conclusions

958 Tree LAI of forest ecosystem has routinely been mapped
 959 based on the empirical relationships between SVI derived from
 960 remote sensing imagery and LAI field measurements. The
 961 suitability of this approach is limited for tree and shrub LAI
 962 mapping in ombrotrophic peatlands, mainly due to the spatially
 963 varying vegetation structure of their multi-layer canopy, which
 964 usually includes a moss ground cover. Additionally, mosses
 965 have spectral characteristics that are significantly different from
 966 vascular plants.

967 Based on a promising approach to map tree LAI in forest
 968 ecosystems using fractions from mixture decomposition with
 969 SMA, we mapped tree and shrub LAI of an ombrotrophic
 970 peatland at the peak growing season. Applying MESMA, an
 971 extension of SMA, to a three-endmember model comprising a
 972 general sunlit vascular plant canopy, *Sphagnum* moss, and
 973 shadow, the widely varying spectral characteristics of *Sphag-*
 974 *num* mosses were taken into account in the mixture decompo-
 975 sition. A slightly higher percentage of pixels of the Mer Bleue
 976 bog were successfully unmixed by our three endmember model
 977 with MESMA than with SMA. Furthermore, mixture decompo-
 978 sition with MESMA reduces the RMSE, mainly in portions

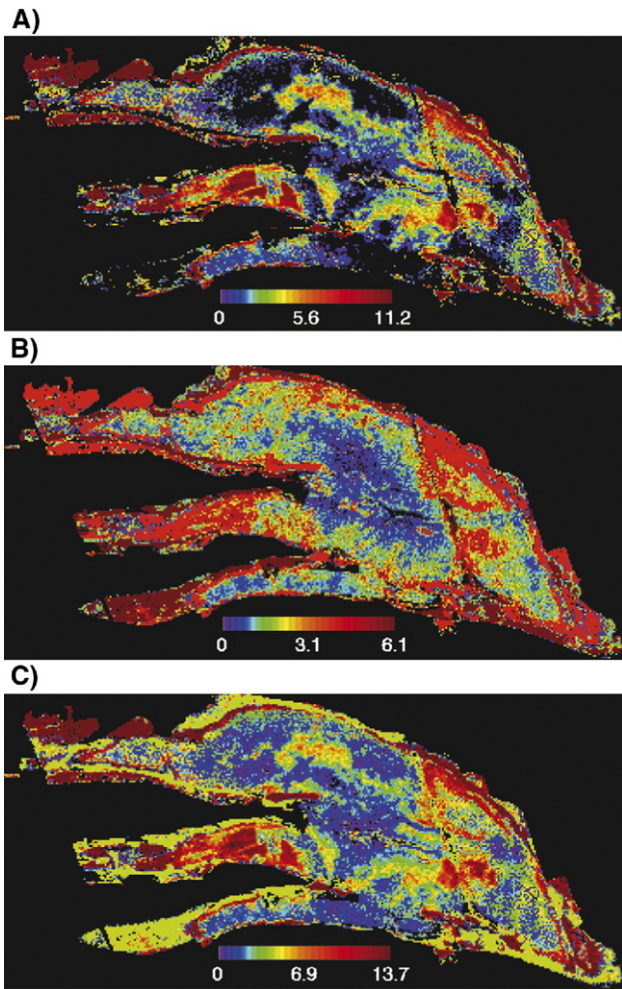


Fig. 15. Mapped LAI for Mer Bleue based on fractions obtained from MESMA and Chen et al. (2002): tree LAI (A), shrub LAI (B), and total LAI (C).

979 of Mer Bleue bog where the shrub canopy is sparse or absent
 980 and the overall pixel spectral signature is mainly controlled by
 981 the spectral characteristics of *Sphagnum* mosses. Thus, it can be
 982 assumed that the fractions obtained from MESMA are more
 983 accurate than the fractions obtained from SMA.

984 The nature of the exponential relationship between shadow
 985 fraction and tree LAI in peatlands shows that a small portion of
 986 the shadow fraction has to be attributed to the shrub canopy.
 987 Validation with LOOC shows that less accurate fractions from
 988 SMA than from MESMA result in weaker predictions of both
 989 tree and shrub LAI.

990 We are confident that our approach developed for the multi-
 991 layer canopy of an ombrotrophic peatland can be used suc-
 992 cessfully to map tree and shrub LAI in similar ecosystems. For
 993 example, another common type of peatland includes fens,
 994 which receive, in addition to precipitation, hydrological inputs
 995 from their surrounding mineral uplands in the form of surface
 996 and subsurface flow (minerotrophic). As a result, fens, com-
 997 monly subdivided into poor and rich fens, are less acidic and
 998 nutrient-rich peatlands, dominated by feather mosses, grami-
 999 noids, shrubs, and coniferous and deciduous trees (Wheeler &
 1000 Proctor, 2000). Future research should investigate the applica-

bility of our approach to the multi-layer canopy of miner-
 otrophic peatlands, and also its applicability to a larger area
 containing both, ombrotrophic and minerotrophic peatlands.
 Furthermore, the applicability of the resulting LAI maps for the
 explicit parameterization of two distinct canopy layers in dis-
 tributed, process-oriented ecosystem models still has to be
 explored.

Acknowledgement

We thank Sylvain Leblanc (Canada Centre for Remote
 Sensing, Ottawa) for sharing his latest version of 4-Scale,
 Marie-Claude Bonneville (McGill University, Montreal) for her
 cattail marsh picture, Prof. Ian Strachan (McGill University,
 Montreal) for providing us with the LAI-2000 instrument, and
 Prof. Jonathan Seaquist (McGill University, Montreal) for
 insightful comments and suggestions. We also thank the three
 anonymous reviewers for their careful reading and helpful
 comments on an earlier draft of this manuscript. The Mer Bleue
 boundary vector dataset was kindly provided by Gershon
 Rother (National Capital Commission, Ottawa). This work was
 supported by the Fluxnet Canada Research Network funded by
 the Natural Science and Engineering Council of Canada, the
 Canadian Foundation of Climate and Atmospheric Sciences and
 BIOCAP Canada.

Appendix A

For 12 tamarack trees we measured height, diameter at breast
 height (DBH), and average branch length at three different
 height levels (top, middle, and bottom), and counted the number
 of branches of the entire tree. For three representative branches
 corresponding to the average length of each height level we
 counted the number of twigs, and measured their lengths and
 radii at the stem and at the end. Based on these measurements
 we calculated the woody surface area (A_W) of each tree as the
 sum of stem surface area (A_S), average branch surface area (A_B),
 and average twig surface area (A_T). A_S and A_T were calculated as
 the lateral surface area of circular cylinders with:

$$A = 2\pi rh \quad (\text{A} - 1)$$

where r is stem radius [m] and an average twig radius of
 0.002 m, respectively, and h is tree height [m] and twig length
 [m], respectively. A_B was calculated by equally dividing the
 total number of branches into the three height levels and
 multiplying the number of branches with an average branch
 surface area of each height level, which was calculated as the
 surface area of truncated cones not including the top and the
 base circles, with:

$$A = \pi(r_1 + r_2)\sqrt{(r_1 - r_2)^2 + h^2} \quad (\text{A} - 2)$$

where r_1 and r_2 are average branch radii [m] at the stem and at
 the end, respectively, and h is average branch length [m] per
 height level of each tree. The calculation of total tree leaf area
 (A_L) is based on a needle-to-woody area ratio ε , which we

1050 calculated based on the 90 tamarack shoot samples collected for
1051 the needle-to-shoot area estimation with:

$$\varepsilon = \frac{\sum A_N}{\sum A_T} \quad (\text{A} - 3)$$

1053 where A_N is half the total needle area (including all sides) in a
1054 shoot [m^2], and A_T is half the total woody area [m^2] of a shoot
1055 sample, i.e. half the surface area of its twig. A_T was calculated
1056 using Eq. (A-1) with the average twig radius of 0.002 m
1057 determined as part of the previous tree woody area calculation,
1058 and the twig length [m] of the respective shoot sample. Based
1059 on Eq. (A-3) we calculated an average value for ε of 11.69. The
1060 total needle surface area of each tree was calculated as the sum
of the top, middle, and bottom level needle surface areas, which
1062 in turn were calculated by multiplying ε with the twig surface
1063 area of the respective height level as determined in the previous
1064 tree woody area calculation. Using A_W and A_N , we calculated an
1065 average value for α in accordance with Kucharik et al. (1998)
1066 with:

$$\alpha = \frac{\sum A_W}{\sum A_W + \sum A_N} \quad (\text{A} - 4)$$

1067

1069 Appendix B

1070 The geometric-optical radiative transfer model 4-Scale
1071 considers the interaction of light with architectural elements
1072 of tree canopies at four different scales: tree groups, tree crowns,
1073 branches, and foliage elements. To simulate the patchiness
1074 usually observed in boreal forests, 4-Scale uses a Neyman type
1075 A distribution, assuming that trees are combined in groups, with
1076 the center of the group entirely contained in quadrats that divide
1077 the simulation domain into smaller areas (Chen & Leblanc,
1078 1997). A geometry-based multiple scattering scheme considers
1079 the scattering of light between all architectural canopy elements
1080 (Chen & Leblanc, 2001).

1081 In our study we parameterized 4-Scale using averaged leaf
1082 scale western larch (*Larix occidentalis*) reflectance and trans-
mittance spectra obtained as part of a previous study (D.A.
1084 Roberts, unpublished data). The leaf scale spectra were mea-
1085 sured using a modified Beckman DK2A with an integrating
1086 sphere attachment designed for measurements of directional
1087 hemispherical transmittance or reflectance. Western larch spec-
1088 tra were collected from needles destructively sampled from the
1089 sunlit portions of lower tree crowns. After collection, needles
1090 were stored cooled and transported to the laboratory for spectral
1091 measurements. Spectra were collected within 48 h of original
1092 collection. Laboratory spectra were collected from needles ar-
1093 ranged on slide mounts with minimal gaps and overlaps as
1094 described by Roberts et al. (2004). Regarding the optical prop-
1095 erties of background, we parameterized 4-Scale using the aver-
1096 age of nine sets of branch scale background reflectance spectra
1097 obtained in this study.

1098 In addition to leaf and branch scale input reflectance spectra,
1099 4-Scale requires several site- and tree architecture specific input
1100 parameters including tree LAI and stand density. To avoid the

arbitrary variation of stand density with increasing tree LAI or
the “growth” of bigger trees with less foliage by keeping stand
density constant with increasing tree LAI, we determined the
empirical relationship between stand density and tree LAI with
unconstrained nonlinear OLS regression analysis for a total of
nine flags of mbt3, mbt4, and mbt5.

Based on the exponential stand density vs. tree LAI
relationship ($R^2=0.62$) we estimated stand densities
corresponding to tree LAI values of 0.1, 0.5, 1.0, 1.5, 2.0,
2.5, and 3.0 (Table B-1). For comparison of simulated shadow
fractions with shadow fractions derived from the subset of the
Landsat TM scene with SMA and MESMA, the simulations
were performed using a SZA corresponding to date and time of
image acquisition and a viewing zenith angle (VZA) of 0° .
Other parameters required by 4-Scale are based on field
observations (stick and crown height, crown radius, and foliage
element size) and measurements (clumping index, needle-to-
shoot area ratio) obtained in this study, or are set following
literature recommendations (number of quadrats, Neyman A
grouping, and repulsion factor that avoids unnatural tree crown
overlapping) after Chen and Leblanc (1997).

Based on the input spectra and the site- and tree architecture
specific input parameters of Table B-1, 4-Scale calculates the
spectral reflectance of the four domain components sunlit and
shaded crown, and sunlit and shaded background, together with
their respective fractions. The overall domain spectral reflectance
is calculated by associating the spectral reflectance of the
domain components with their fractions according to Eq. (3)
without the residual error.

Table B-1: 4-Scale parameterizations used to investigate the
nature of the empirical relationship between shadow fraction
and tree LAI for Mer Bleue bog

	LAI	0.1	0.5	1	1.5	2	2.5	3	
Site	Size	900	900	900	900	900	900	900	1145
parameters	Stand	64	64	153	294	354	380	391	1146
	density [trees/900 m^2]								1149
Tree	# Quadrats [-]	5	5	5	5	5	5	5	1152
	Neyman A grouping [-]	2	2	2	2	2	2	2	1153
Other	SZA [$^\circ$]	43	43	43	43	43	43	43	1158
	VZA [$^\circ$]	0	0	0	0	0	0	0	1160
	Stick height [m]	0.2	0.2	0.2	0.1	0.1	0.1	0.1	1162
	Crown height [m]	1.7	1.7	1.7	1.1	1.1	1.1	1.1	1164
	Crown radius [m]	0.7	0.4	0.4	0.3	0.3	0.3	0.3	1166
	Clumping index [-]	0.87	0.87	0.87	0.87	0.87	0.87	0.87	1168
	Apex angle [$^\circ$]	13	13	13	13	13	13	13	1170
	Needle-to-shoot area ratio [-]	1.41	1.41	1.41	1.41	1.41	1.41	1.41	1172
	Foliage element size [m]	0.05	0.05	0.05	0.05	0.05	0.05	0.05	1175
	Repulsion factor	0.5	0.5	0.5	0.5	0.5	0.5	0.5	1179

References

- Adams, J. N., Smith, M. O., & Gillespie, A. R. (1993). Imaging spectrometry: Interpretation based on spectral mixture analysis. In C. M. Pieters, & P. A. J.

- 1185 Englert (Eds.), *Remote geochemical analysis: Elemental and mineralogical*
 1186 *composition* (pp. 145–166). Cambridge, England: Press Syndicate of
 1187 University of Cambridge.
- 1188 Baldocchi, D., Kelliher, F. M., Black, T. A., & Jarvis, P. G. (2000). Climate and
 1189 vegetation controls on boreal zone energy exchange. *Global Change Biology*,
 1190 6, 69–83.
- 1191 Ballantine, J. -A. C., Okin, G. S., Prentiss, D. E., & Roberts, D. A. (2005).
 1192 Mapping African landforms using continental scale unmixing of MODIS
 1193 imagery. *Remote Sensing of Environment*, 97, 470–483.
- 1194 Barr, A. G., Black, T. A., Hogg, E. H., Kljun, N., Morgenstern, K., & Nescic, Z.
 1195 (2004). Inter-annual variability in the leaf area index of a boreal aspen–
 1196 hazelnut forest in relation to net ecosystem production. *Agricultural and*
 1197 *Forest Meteorology*, 126, 237–255.
- Berterretche, M., Hudak, A. T., Cohen, W. B., Maierperger, T. K., Gower, S. T.,
 1199 & Dungan, J. (2005). Comparison of regression and geostatistical methods
 1200 for mapping leaf area index (LAI) with Landsat ETM+ over a boreal forest.
 1201 *Remote Sensing of Environment*, 96, 49–61.
- 1202 Boardman, J. W., Kruse, F. A., & Green, R. O. (1995). Mapping target signatures
 1203 via partial unmixing of AVIRIS data. *Summaries, 5th JPL Airborne Earth*
 1204 *Science Workshop, Vol. 1* (pp. 23–26) Pasadena, CA: Jet Propulsion Laboratory
 1205 (JPL Publications 95-1).
- 1206 Brown, L., Chen, J. M., Leblanc, S. G., & Cihlar, J. (2000). A shortwave infrared
 1207 modification to the Simple Ratio for LAI retrieval in boreal forests: An image
 1208 and model analysis. *Remote Sensing of Environment*, 71, 16–25.
- 1209 Bryant, R. G. (1996). Validated linear mixture modelling of Landsat TM data for
 1210 mapping evaporate minerals on a playa surface: Methods and applications.
 1211 *International Journal of Remote Sensing*, 17, 315–330.
- 1212 Bryant, R. G., & Baird, A. J. (2003). The spectral behaviour of *Sphagnum* canopies
 1213 under varying hydrological conditions. *Geophysical Research Letters*, 30,
 1214 1134–1138.
- 1215 Bubier, J. L., Barrett, N. R., & Crill, P. M. (1997). Spectral reflectance mea-
 1216 surements of boreal wetland and forest mosses. *Journal of Geophysical*
 1217 *Research*, 102(D24), 29483–29494.
- 1218 Chen, J. M. (1996). Optically-based methods for measuring seasonal variation of
 1219 leaf area index in boreal conifer stands. *Agricultural and Forest Meteorology*,
 1220 80, 153–163.
- 1221 Chen, J. M., & Black, T. A. (1992). Defining leaf area index for non-flat leaves.
 1222 *Plant, Cell & Environment*, 15, 421–429.
- 1223 Chen, J. M., & Cihlar, J. (1995). Plant canopy gap size analysis theory for
 1224 improving optical measurements of leaf area index. *Applied Optics*, 34,
 1225 6211–6222.
- 1226 Chen, J. M., & Cihlar, J. (1996). Retrieving leaf area index of boreal conifer forests
 1227 using Landsat TM images. *Remote Sensing of Environment*, 55, 153–162.
- 1228 Chen, J. M., Govind, A., Sonnentag, O., Zhang, Y., Barr, A., & Amiro, B.
 1229 (2006). Leaf area index measurements at Fluxnet Canada forest sites, FCNR
 1230 special issue. *Agricultural and Forest Meteorology*, 140, 257–268.
- 1231 Chen, J. M., & Leblanc, S. G. (1997). A 4-Scale bidirectional reflection model
 1232 based on canopy architecture. *IEEE Transactions on Geoscience and*
 1233 *Remote Sensing*, 35, 1316–1337.
- 1234 Chen, J. M., & Leblanc, S. G. (2001). Multiple scattering scheme useful for
 1235 geometric optical modelling. *IEEE Transactions on Geoscience and Remote*
 1236 *Sensing*, 39, 1061–1071.
- 1237 Chen, J. M., Pavlic, G., Brown, L., Cihlar, J., Leblanc, S. G., White, H. P., et al.
 1238 (2002). Derivation and validation of Canada-wide coarse-resolution leaf
 1239 area index using high-resolution satellite imagery and ground measure-
 1240 ments. *Remote Sensing of Environment*, 80, 165–184.
- 1241 Chen, J. M., Rich, P. M., Gower, S. T., Norman, J. M., & Plummer, S. (1997).
 1242 Leaf area index of boreal forests: Theory, techniques, and measurements.
 1243 *Journal of Geophysical Research*, 102(D24), 29429–29443.
- 1244 Cohen, W. B., Maierperger, T. K., Gower, S. T., & Turner, D. P. (2003). An
 1245 improved strategy for regression of biophysical variables and Landsat ETM+
 1246 data. *Remote Sensing of Environment*, 84, 561–571.
- 1247 Deering, D. W., (1978). Rangeland reflectance characteristics measured by
 1248 aircraft and spacecraft sensors. PhD dissertation, Texas A & M University,
 1249 College Station, TX, 338 pp.
- 1250 Dennison, P. E., Charoensiri, K., Roberts, D. A., Peterson, S. H., & Green, R. O.
 1251 (2006). Wildfire temperature and land cover modeling using hyperspectral
 1252 data. *Remote Sensing of Environment*, 100, 212–222.
- Dennison, P. E., & Roberts, D. A. (2003). Endmember selection for multiple
 1253 endmember spectral mixture analysis using endmember average RMSE.
 1254 *Remote Sensing of Environment*, 87, 123–135.
- Dennison, P. E., & Roberts, D. A. (2003). The effects of vegetation phenology
 1255 on endmember selection and species mapping in Southern California
 1256 Chaparral. *Remote Sensing of Environment*, 87, 295–309.
- Eklundh, L., Hall, K., Eriksson, H., Ardö, J., & Pilesjö, P. (2003). Investigating the
 1257 use of Landsat thematic mapper data for estimation of forest leaf area index in
 1258 southern Sweden. *Canadian Journal of Remote Sensing*, 29, 349–362.
- ENVI. (2004). *Environment for visualizing images. Image analysis software*
 1261 *manual (CD)*. Boulder, Colorado, USA: Research Systems.
- Frolking, S., Roulet, N. T., Moore, T. R., Lafluer, P. M., Bubier, J. L., & Crill, P. M.
 1262 (2002). Modeling seasonal to annual carbon balance of Mer Bleue bog, Ontario,
 1263 Canada. *Global Biogeochemical Cycles*, 16. doi:10.1029/2001GB001457
- Gorham, E. (1991). Northern peatlands: Role in the carbon-cycle and probable
 1264 responses to climatic warming. *Ecological Applications*, 1, 182–195.
- Gower, S. T., & Richards, J. H. (1990). Larches: Deciduous conifers in an
 1265 evergreen world. *BioScience*, 40, 818–826.
- Green, A. A., Berman, M., Switzer, P., & Craig, M. D. (1988). A transformation
 1266 for ordering multispectral data in terms of image quality with implications
 1267 for noise removal. *IEEE Transactions on Geoscience and Remote Sensing*,
 1268 26, 65–74.
- Hall, R. J., Davidson, D. P., & Peddle, D. R. (2003). Ground and remote sensing of
 1269 leaf area index Rocky Mountain forest stands, Kananaskis, Alberta. *Canadian*
 1270 *Journal of Remote Sensing*, 29, 411–427.
- Hall, F. G., Shimabukuro, Y. E., & Huemmerich, K. F. (1995). Remote sensing
 1271 of forest biophysical structure using mixture decomposition and geometric
 1272 reflectance models. *Ecological Applications*, 5, 993–1013.
- Harris, A., Bryant, R. G., & Baird, A. J. (2005). Detecting near-surface moisture
 1273 stress in *Sphagnum* spp. *Remote Sensing of Environment*, 97, 371–381.
- Harris, A., Bryant, R. G., & Baird, A. J. (2006). Mapping the effects of water
 1274 stress on *Sphagnum*: Preliminary observations using airborne remote
 1275 sensing. *Remote Sensing of Environment*, 100, 363–378.
- Heinz, D. C., & Chang, C. -I. (2001). Fully constrained least square linear spectral
 1276 mixture analysis method for material quantification in hyperspectral imagery.
 1277 *IEEE Transactions on Geoscience and Remote Sensing*, 39, 529–545.
- Hu, B., Miller, J. R., Chen, J. M., & Hollinger, A. (2004). Retrieval of canopy
 1278 leaf area index in the BOREAS flux tower sites using linear spectral mixture
 1279 analysis. *Remote Sensing of Environment*, 89, 176–188.
- Isaaks, E. H., & Srivastava, R. M. (1989). *An introduction to applied geostatistics*.
 1280 New York, USA: Oxford University Press.
- Johnson, J. R., Staid, M. L., Titus, T. N., & Becker, K. (2006). Shocked
 1281 plagioclase signatures in Thermal Emission Spectrometer data of Mars.
 1282 *Icarus*, 180, 60–74.
- Jordan, C. F. (1969). Derivation of leaf area index from quality of light on the
 1283 forest floor. *Ecology*, 50, 663–666.
- Kucharik, C. J., Norman, J. M., & Gower, S. T. (1998). Measurements of branch
 1284 area and adjusting leaf area index indirect measurements. *Agricultural and*
 1285 *Forest Meteorology*, 91, 69–88.
- Kruse, F. A., Lefkoff, A. B., Boardman, J. W., Heidebrecht, K. B., Shapiro, A. T.,
 1286 Barloon, J. P., et al. (1993). The Spectral Image-Processing System (Sips) —
 1287 interactive visualization and analysis of imaging spectrometer data. *Remote*
 1288 *Sensing of Environment*, 44, 145–163.
- Lafluer, P. M., Hember, R. A., Admiral, S. W., & Roulet, N. T. (2005). Annual
 1289 and seasonal variability in evapotranspiration and water table at a shrub-
 1290 covered. *Hydrological Processes*, 19, 3533–3550.
- Li, L., & Mustard, J. F. (2003). Highland contamination in lunar mare soils:
 1291 Improved mapping with multiple end-member spectral mixture analysis.
 1292 *Journal of Geophysical Research*, 108(E6). doi:10.1029/2002JE001917.5033
- Liu, J., Chen, J. M., Cihlar, J., & Park, W. M. (1997). A process-based boreal
 1293 ecosystem productivity simulator using remote sensing inputs. *Remote*
 1294 *Sensing of Environment*, 62, 158–175.
- Moore, T. R., Bubier, J. L., Frolking, S. E., Lafluer, P. M., & Roulet, N. T.
 1295 (2002). Plant biomass and production and CO₂ exchange in an ombrotrophic
 1296 bog. *Journal of Ecology*, 90, 25–36.
- Moore, T. R., Roulet, N. T., & Waddington, J. M. (1998). Uncertainty in
 1297 predicting the effect of climatic change on the carbon cycling of Canadian
 1298 peatlands. *Climatic Change*, 40, 229–245.

- 1321 Norman, J., & Welles, J. (1991). Instruments for indirect measurements of
1322 canopy architecture. *Agronomy Journal*, 82, 818–825.
- 1323 Okin, G. S., Roberts, D. A., Murray, B., & Okin, W. J. (2001). Practical limits on
1324 hyperspectral vegetation discrimination in arid and semiarid environments.
1325 *Remote Sensing of Environment*, 77, 212–225.
- 1326 Olaczek, R. (1986). Outline of larch ecology and phytocenology. In S. Bialobok
1327 (Ed.), *Larch (Larix Mill.)* (pp. 381–440). Warsaw, Poland: PWN-Publishers.
- 1328 Payette, S., & Rochefort, L. (2001). *Écologie des tourbières du Québec-*
1329 *Labrador. Les Presses de l'Université Laval, Sainte-Foy, Canada.*
- 1330 Painter, T. H., Dozier, J., Roberts, D. A., Davis, R. E., & Green, R. O. (2003).
1331 Retrieval of subpixel snow-covered area and grain size from imaging
1332 spectrometer data. *Remote Sensing of Environment*, 85, 64–77.
- 1333 Peddle, D. R., Hall, F. G., & LeDrew, E. F. (1999). Spectral mixture analysis and
1334 geometric-optical reflectance modeling of boreal forest biophysical
1335 structure. *Remote Sensing of Environment*, 67, 288–297.
- 1336 Petrou, M., & Foschi, P. G. (1999). Confidence in linear spectral unmixing of
1337 single pixels. *IEEE Transactions on Geoscience and Remote Sensing*, 37,
1338 624–626.
- 1339 Rashed, T., Weeks, J. R., Roberts, D. A., Rogan, J., & Powell, R. (2003). Measuring
1340 the physical composition of urban morphology using multiple endmember
1341 spectral mixture models. *Photogrammetric Engineering and Remote Sensing*,
1342 69, 1011–1020.
- 1343 Roberts, D. A., Dennison, P. E., Gardner, M., Hetzel, Y., Ustin, S. L., & Lee, C.
1344 (2003). Evaluation of the potential of Hyperion for fire danger assessment by
1345 comparison to the Airborne Visible/Infrared Imaging Spectrometer. *IEEE*
1346 *Transactions on Geoscience and Remote Sensing*, 41, 1297–1310.
- 1347 Roberts, D. A., Gardner, M., Church, R., Ustin, S., Scheer, G., & Green, R. O.
1348 (1998). Mapping Chaparral in the Sierra Monica Mountains using multiple
1349 endmember spectral mixture models. *Remote Sensing of Environment*, 16,
1350 2165–2185.
- 1351 Roberts, D. A., Smith, M. O., & Adams, J. B. (1993). Green vegetation,
1352 nonphotosynthetic vegetation, and soils in AVIRIS data. *Remote Sensing of*
1353 *Environment*, 44, 255–269.
- 1354 Roberts, D. A., Ustin, S. L., Ogunjemiyo, S., Greenberg, J., Dobrowski, S. Z.,
1355 Chen, J., et al. (2004). Spectral and structural measures of northwest forest
1356 vegetation at leaf to landscape scales. *Ecosystems*, 7, 545–562.
- 1392
- Roulet, N. T., Lafleur, P., Richard, P. J. H., Moore, T. R., Humphreys, E., & Bubier, J. (2006). Contemporary carbon balance and late Holocene carbon accumulation in a northern peatland. *Global Change Biology*, 12, 1–15. doi:10.1111/j.1365-2486.2006.01292.x
- Schweik, C. M., & Green, G. M. (1999). The use of spectral mixture analysis to study human incentives, action, and environmental outcomes. *Social Science Computer Review*, 17, 40–63.
- Song, T. (2005). Spectral mixture analysis for subpixel vegetation fractions in the urban environment: How to incorporate endmember variability? *Remote Sensing of Environment*, 95, 248–263.
- Sonnentag, O., Talbot, J., Chen, J. M., & Roulet, N. T. (accepted for publication). Using direct and indirect measurements of leaf area index to characterize the shrub canopy in an ombrotrophic peatland. *Agricultural and Forest Meteorology*.
- Tarnocai, C., Kettles, I. M., & Lacelle, B., (2000). *Peatlands of Canada Map*. Geological Survey of Canada, Open File 3834. Scale 1: 6 500 000. Natural Resources Canada, Ottawa.
- Tompkins, S., Mustard, J. F., Pieters, C. M., & Forsyth, D. W. (1997). Optimization of endmembers for spectral mixture analysis. *Remote Sensing of Environment*, 59, 472–489.
- Theseira, M. A., Thomas, G., Taylor, J. C., Gemell, F., & Varjo, J. (2003). Sensitivity of mixture modelling to end-member selection. *International Journal of Remote Sensing*, 24, 1559–1575.
- Turunen, J., Tomppo, E., Tolonen, K., & Reinikainen, A. (2002). Estimating carbon accumulation rates of undrained mires in Finland — application to boreal and subarctic regions. *Holocene*, 12, 69–80.
- Vermote, E. F., Tanré, D., Deuzé, J. L., Herman, M., & Morcrette, J. -J. (1997). Second simulation of the satellite signal in the solar spectrum, 6S: An overview. *IEEE Transactions on Geoscience and Remote Sensing*, 35, 675–686.
- Wheeler, B. D., & Proctor, M. C. F. (2000). Ecological gradients, subdivisions, and terminology of North-West European mires. *Journal of Ecology*, 88, 187–203.
- Wu, C., & Murray, A. T. (2003). Estimating impervious surface distribution by spectral mixture analysis. *Remote Sensing of Environment*, 84, 493–505.